Estimation of Return Levels for Extreme Skew Surge Coastal Flooding Events in the Delaware and Chesapeake Bays for 1980 – 2019

John A. Callahan[1*], Daniel J. Leathers[2]

[1]Delaware Geological Survey, Department of Geography and Spatial Sciences, University of Delaware, Newark, Delaware, USA

[2]Department of Geography and Spatial Sciences, Center for Environmental Monitoring & Analysis, University of Delaware, Newark, Delaware, USA

*** Correspondence:**
Corresponding Author
john.callahan@udel.edu

Keywords: extreme value analysis, storm surge, coastal flooding, flood risk, Mid-Atlantic, tidal analysis

Abstract

Extreme storm surges can overwhelm many coastal flooding protection measures in place and cause severe damages to private communities, public infrastructure, and natural ecosystems. In the US Mid-Atlantic, a highly developed and commercially active region, coastal flooding is one of the most significant natural hazards and a year-round threat from both tropical and extra-tropical cyclones. Mean sea levels and high-tide flood frequency has increased significantly in recent years, and major storms are projected to increase into the foreseeable future. We estimate extreme surges using hourly water level data and harmonic analysis for 1980-2019 at 12 NOAA tide gauges in and around the Delaware and Chesapeake Bays. Return levels (RLs) are computed for 1.1, 3, 5, 10, 25, 50, and 100-year return periods using stationary extreme value analysis on detrended skew surges. Two traditional approaches are investigated, Block Maxima fit to General Extreme Value distribution and Points-Over-Threshold fit to Generalized Pareto distribution, although with two important enhancements. First, the GEV r-largest order statistics distribution is used; a modified version of the GEV distribution that allows for multiple maximum values per year. Second, a systematic procedure is used to select the optimum value for r (for the BM/GEVr approach) and the threshold (for the POT/GP approach) at each tide gauge separately. RLs have similar magnitudes and spatial patterns from both methods, with BM/GEVr resulting in generally larger 100-yr and smaller 1.1-yr RLs. Maximum values are found at the Lewes (Delaware Bay) and Sewells Point (Chesapeake Bay) tide gauges, both located in the southwest region of their respective bays. Minimum values are found toward the central bay regions. In the Delaware Bay, the POT/GP approach is consistent and results in narrower uncertainty bands whereas the results are mixed for the Chesapeake. Results from this study aim to increase reliability of projections of extreme water levels due to extreme storms and ultimately help in long-term planning of mitigation and implementation of adaptation measures.

1 Introduction

Coastal flooding poses the greatest threat to human life and is often the source of much of the damage resulting from the storm surge and waves of coastal weather systems (Blake and Gibney, 2011; Rappaport, 2014; Chippy and Jawahar, 2018; Weinkle et al., 2018). Relative sea-level rise (SLR) rates and high-tide flooding frequency and magnitude along the US East Coast have increased in recent decades and are expected to continue increasing into the near future (Sweet et al., 2018; Sweet et al., 2017a; Oppenheimer et al., 2019) with recent studies estimating mean sea levels are rising faster than predicted (Grinsted and Christensen, 2021). The US Mid-Atlantic coast is noted for especially high SLR rates (Sallenger et al., 2012; Kopp, 2013; Boon et al., 2018; Pieutsch 2018) and states and counties in this region view coastal flooding as one of their most severe and pervasive natural hazards to prepare for (Callahan et al., 2017; Boesch et al., 2018; Dupigny-Giroux et al., 2018). Increases in sea levels lead directly to higher frequencies of coastal flooding from high tides as well as minor and major coastal storms (Lin et al., 2016; Dahl et al., 2017; Rahmstorf, 2017; Sweet et al., 2017b, Garner et al., 2017; Muis et al., 2020; Taherkhani et al., 2020).

Many of the largest coastal flooding events along the US Mid-Atlantic coast are caused by tropical cyclones (TCs), most notably Hurricanes Isabel in 2003 and Sandy in 2012, TCs can account for 40-60% of the top 10 flood events with higher relative percentages in the southern part of the region (Booth et al., 2016). For both the US Atlantic and Gulf Coasts, tropical cyclones are the costliest and most damaging weather and climate event (Smith, 2021). Under current global warming scenarios, atmospheric water vapor content and sea-surface temperatures (SSTs) in the North Atlantic Ocean are projected to increase, leading to an increase in the number of severe tropical cyclones, decreases in the forward translational speed, increases in wind speed, and increases in the rate of intensification, especially near the coasts (Kossin et al., 2017; Kossin, 2018; Knutson et al., 2019; Knutson et al., 2020; Murakami et al., 2020; Yang et al., 2020; Wang and Toumi, 2021).

Although TCs may gather much of the attention, the threat of major coastal flooding in the region is year-round (Dupigny-Giroux et al., 2018). East Coast winter storms, surface high pressure systems (fall to spring), and tropical systems (summer to fall) regularly impact the region (Hirsch et al, 2000; Thompson et al., 2013). Non-tropical systems are collectively termed as extratropical cyclones (ETCs), as there is often a closed isobar of low-pressure nearby; approximately 32 days per year a closed isobar of low-pressure was present off the shore of the Delmarva Peninsula from 1945 – 2019 (Leathers et al., 2013).

Mid-Atlantic weather in the winter and spring is often dictated by the relative position of troughs in the westerly polar jet stream, directing low-pressure centers to travel northeastward up the coast over warmer waters, often intensifying into strong nor-easter storms. The Ash Wednesday Storm of March 1962, one of the most destructive storms ever to hit the region (Morton et al., 2009), was blocked by an upper-level ridge to the east in the North Atlantic Ocean, which caused the storm to stall and continuously pile up water levels though onshore winds for 5 tidal cycles. Winds were amplified by an enhanced pressure gradient due to a surface high-pressure system to the north. As well, water levels were amplified as this storm occurred during a perigean spring tide a couple of weeks before the spring equinox. This was the storm of record (with respect to coastal flooding at the NOAA Lewes tide gauge) for 54 years until broken by a more classic nor'easter in January 2016. Although this storm also deeply intensified offshore and occurred during a spring tide, it moved unimpeded up the coast and lasted the more typical 2-3 tidal cycles. Peak water levels occurred at its first high tide and easterly winds did not persist long. With the aid of 54 years of sea-level rise, it set

the record of highest water levels ever recorded at the NOAA Lewes tide gauge, although caused significantly less damage than the 1962 storm.

The Mid-Atlantic lies in a climatic transition zone, between continental and marine climate types, split in the Fourth National Climate Assessment between the Northeast and the Southeast Regions (Jay et al., 2018). Along with major TCs, SSTs, and sea levels, the intensity and winds of ETCs and associated beach erosion and other damages due to coastal flooding, are all projected to increase due to climate change, however projections of landfalling TCs and ETC storm tracks due to changing synoptic atmospheric patterns (i.e., "storminess") in the Mid-Atlantic is inconclusive (Hall et al., 2016; Mawdsley and Haigh, 2016; Dupigny-Giroux et al., 2018). Studies have found that US East Coast sea levels vary with synoptic oscillations (Wahl et al., 2015; Colle et al., 2015; Sweet et al., 2020), leading Rashid et al. (2019) to conclude that interannual and multi-decadal variability of extreme storm surge in the Mid-Atlantic was in a transition zone between more clear relationships found in the Northeast and Southeast portions of the US Atlantic Coast.

Water levels in the Delaware and Chesapeake Bays, two of the largest estuaries in the US located in the Mid-Atlantic, have been well monitored for several decades by high-quality tide-gauge networks, well-suited for climate studies (Holgate et al., 2013; Sweet et al., 2017a; NOAA PORTS, 2020; NOAA NWLON, 2020). This highly developed, economically critical region includes many commercial industries, vast amounts of public and private infrastructure, and provides important ecosystem services (Sanchez et al., 2012; PDE 2017; Chesapeake Bay Program, 2020). Impacts and costs associated with coastal flooding are highly dependent upon both the natural and social vulnerability, the amount of exposure, and adaptation measures in place (Hallegatte et al., 2013; Hinkel et al., 2014).

Extreme coastal flooding can overwhelm many protections in place and can have profound negative effects in this region, such as saltwater overtopping into wetland forests and low-lying agricultural fields; physical damage of surge and waves on homes and businesses; severe beach erosion; decrease of coastal tourism; degradation of freshwater wetlands; and flooding of roads and personal property putting human life at risk. Extreme events often include multiple hazards that compound the damage, leading to their net impact to be greater than the sum of its parts (Kopp et al., 2017; Moftakhari et al., 2017). In 2020, there were 22 weather and climate disasters in the US with total cost estimates over $1 billion each, most of which involved coastal flooding (Smith, 2021). Estimating frequency and severity of extreme coastal flooding is difficult as, by definition, these events do not occur often. This lack of observational data makes it difficult to develop robust statistical or physical predictive models at the usual level of confidence although planning and design for extremes are essential to avoid the most severe consequences (Walton, 2000; Calafat et al., 2020).

A common method to estimate the frequency of extremes (i.e., extreme value analysis, or EVA) is by assuming the largest values from an observational record can be modeled by a statistical distribution distinct from the parent distribution. Two families of extreme value distributions have been shown to model extreme values well: the Generalized Extreme Value (GEV) distribution and the Generalized Pareto (GP) distribution (Coles, 2001). The GEV distribution can be fit to the set of maximum values of discrete, non-overlapping blocks within a time series, such as annual maximum values; this is termed the Block Maxima (BM) approach. Data points using this approach are evenly distributed over time, however, non-extreme data points from years with abnormally low values may be forced into the model fit, biasing the results. In contrast, the GP distribution can be fit to the upper tail of the parent distribution, i.e., the set of values that are greater than a pre-selected threshold; this is termed the Points-Over-Threshold (POT) approach (Coles, 2001). POT is a more natural

interpretation of modeling extreme results although the data points may come in temporal clusters and selection of a threshold is subjective. Which approach is considered "better" is non-trivial and dependent upon the parent distribution of the data, time period, sample size, as well as the metric used to measure each model performance (Walton 2000; Wong et al., 2020).

The overall focus of the current study is to conduct EVA on coastal flooding due to storms in the Mid-Atlantic region. Numerous studies have performed EVA of total water levels (TWL) using a variety of methods along the US coastlines; a few recent examples can be found in Wahl (2017), Kopp et al. (2019), Oppenheimer et al. (2019), Wong et al. (2020), and Sweet et al. (2020). TWL is an important measure of flooding, however, it is inherently influenced by location-specific tidal ranges and timing of the storm event relative to the phase of the tide. Storm surge, computed as the maximum difference between TWL and predicted tide, often called the maximum non-tidal residual (NTR), is more closely associated with the characteristics of a storm. EVA of storm surge as the maximum NTR have been performed along the US Atlantic coasts using both the BM/GEV (Grinsted et al., 2012; Sweet et al., 2014) and POT/GP (Bernier and Thompson, 2006; Tebaldi et al., 2012; USACE 2014; Booth et al., 2016; Hall et al., 2016) approaches, or comparing the two methods (Walton 2000; Wong et al., 2020). EVA methods such as bootstrap simulations (Garner et al., 2017) or global modelling (Muis et al., 2020) on storm surge have also been investigated.

Skew surge, however, is arguably a more accurate measure of storm surge and most appropriate for long-term planning and estimating extreme flood levels solely due to storms. It is defined as the difference between the maximum observed TWL and the maximum predicted tide during a tidal cycle, even if the observed and predicted tidal peaks are offset (i.e., skewed) from each other (Pugh and Woodworth, 2014). It represents the meteorologically-forced increase of water levels more clearly separated from the astronomically forced-tides and tide-surge interactions (Batstone, 2013; Mawdsley and Haigh, 2016; Williams et al., 2016; Stephens et al., 2020). Skew surge levels are consistently less than the measures of maximum NTR up to 30% (Hall et al., 2016; Callahan et al., 2021), and less susceptible to timing errors and potential complex hydrodynamics of tide-surge interactions. There have been very few studies on the EVA of skew surge in the Mid-Atlantic. Mawdsley and Haigh (2016) analyzed long term trends of skew surge and Williams et al. (2016) investigated tide-skew surge independence, but only a few Mid-Atlantic tide gages were included in those analyses and neither performed traditional EVA on skew surges. Callahan et al. (2021) computed skew surge at the same tide gauges as the current study but only analyzed tropical cyclones.

Specific goals of this study are two-fold. First goal is to estimate extreme skew surges within the Delaware and Chesapeake Bays and investigate sub-bay geographic differences. Many tide gauges in these bays started collecting data in the late 1970s and only recently has there been sufficient geographic coverages of gauges with records of at least 40 years of continuous hourly data. Second goal is to modify the two common traditional EVA approaches by implementing objective criteria for model parameter selection, and then compare results of each. The BM approach is enhanced to incorporate the GEVr distribution, a slightly modified form of the GEV distribution. GEVr approach allows for the inclusion of multiple values (the r-largest orders) per year instead of only the annual maximum (see Section 2.5 for details), addressing the biggest issue with the traditional BM approach, i.e., the small number of data incorporated in the model.

The paper is structured by first describing how skew surge is computed from hourly tide gauge measurements. Statistical methods of BM/GEVr and POT/GP approaches are then briefly described with focus on a systematic procedure for selecting the optimum r (BM/GEVr) and threshold

(POT/GP). Mean skew surges throughout the study region are then summarized and compared against total water levels and tidal datums. Results of model parameter selection and return levels for 1.1-yr to 100-yr return periods using both approaches are discussed, with emphasis on the differences on magnitude and geography. It is not the intent of this paper to determine the "best" EVA approach to use in all cases, but rather to better understand the differences between them and to increase reliability of projections of extreme water levels due to storms, ultimately helping in long-term planning of mitigation and implementation of adaptation measures.

2 Materials and Methods

2.1 Study Region

The Delmarva Peninsula, located in the US Mid-Atlantic, is flanked on both sides by the Delaware and Chesapeake Bays (Figure 1). Tidal water levels and storm surges are influenced by the geomorphological environment, geometry of the coastline, bathymetry, bottom friction/dissipation effects, and reflection of the wave near the head of the bay (Lee et al., 2017). Storm surge is additionally influenced by storm size and direction of travel, duration, atmospheric pressure, wind speed and wind direction relative to the coastline (Ellis and Sherman, 2015). The Delaware Bay has a classical funnel shape, with pockets of deep scour in the wider lower bay, amplifying tidal range and storm surge in the northern regions (Wong and Münchow, 1995; Lee et al., 2017; Ross et al, 2017). The Chesapeake Bay, by contrast is longer, shallower, exhibits a more dendritic tributary landscape, and its lowest tidal ranges are towards the center (Zhong and Li, 2006; Lee at al., 2017; Ross et al., 2017). Although coastal storms threaten the region year-round, mean water levels follow a bimodal seasonal distribution with the maximum in fall (October) and secondary maximum in late spring (May-Jun), primarily caused by periodic fluctuations in atmospheric weather systems and coastal water steric effects (NOAA CO-OPS, 2020a). The largest coastal flood events typically occur either during peak hurricane season (Sept – Nov) or during the winter/early spring from nor'easters (Dec – Mar).

2.2 Water Level Data and Computation of Skew Surge

Tide gauges selected for this study were limited to NOAA operational tide gauges in and immediately around the Delaware and Chesapeake Bays. Requirements were that each gauge maintained nearly continuous record of hourly water levels for the time period 1980 – 2019, evenly located throughout the region, a set of harmonic constituents identified for making tidal predictions, and a vertical tidal datum conversion factor to North American Vertical Datum of 1988 (NAVD88). In all, 12 gauges were selected; 5 associated with the Delaware Bay and 7 with the Chesapeake (Figure 1; Table 1). All selected gauges are part of NOAA NWLON and PORTS networks.

Table 1. *Tide gauges used in the current study. Bay denotes if either Delaware or Chesapeake Bay is most closely associated with the gauge. Number of data gaps and percent hourly data based upon time period 1980 – 2019. Large data gaps represent continuous gaps of 745 hours or more.*

Station	Code	NOAA ID	Bay	Coordinates	Large Data Gaps	Percent Hourly
Philadelphia	PHL	8545240	Delaware	39.933000, -75.142667	0	99.23%
Reedy Point	RDY	8551910	Delaware	39.558333, -75.573333	5	95.61%
Lewes	LEW	8557380	Delaware	38.781667, -75.120000	0	99.73%
Cape May	CAP	8536110	Delaware	38.968333, -74.960000	2	98.35%
Atlantic City	ATL	8534720	Delaware	39.356667, -74.418333	2	98.08%
Baltimore	BAL	8574680	Chesapeake	39.266667, -76.580000	0	99.66%
Annapolis	ANN	8575512	Chesapeake	38.983333, -76.481667	1	98.70%
Cambridge	CAM	8571892	Chesapeake	38.571667, -76.061667	1	98.84%
Lewisetta	LWS	8635750	Chesapeake	37.995000, -76.465000	2	98.72%
Kiptopeke	KIP	8632200	Chesapeake	37.165000, -75.988333	0	99.78%
Sewells Point	SEW	8638610	Chesapeake	36.946667, -76.330000	0	100.00%
Wachapreague	WAC	8631044	Chesapeake	37.608333, -75.685000	6	89.30%

Hourly and High/Low water level data were obtained from the NOAA Center for Operational Oceanographic Products and Services (NOAA CO-OPS, 2020b). High/Low data represent the exact time and magnitude of each Higher-High, High, Low, and Lower-Low tidal peak. Hourly data represent the observed water level on each hour (e.g., 21:00, 22:00). The 40 years of hourly data at each gauge were manually inspected for errors and inconsistencies. A few small data clusters (of 2 – 16 hours) within larger gaps of missing data were removed (on seven occasions across all gauges) and small data gaps of 1-2 hours (less than 10 across all gauges) were filled using linear interpolation. Table 1 lists the number of data gaps that spanned 745 hours (approximately 1 month) or greater as well as the percentage of valid hourly data points used in the analysis. Wachapreague had the largest amount of missing data due to a 2.5-year period (200511 – 200804) when valid Hourly and High/Low data were unavailable.

Skew surge was computed at each tidal peak over 1980 – 2019 using modeled predicted time series as reference. Total count was a maximum of 28,231 tidal peaks over the study time period, less any missing data. The observed maximum TWL at each peak was extracted from the High/Low dataset; the maximum hourly value was used if High/Low data were not available. The observed and predicted peaks were aligned within +/- 3 hours of each other, which was extended to +/- 6 hours if no High/Low or TWL peak alignment was found, such as due to prolonged surge; this occurred for < 100 peaks over the entire study time period and only for gauges in the Chesapeake Bay.

Predicted tides were generated through Harmonic Analysis (HA) based on hourly water levels. The HA incorporated 37 tidal constituents defined by NOAA for their official tide predictions in this region (NOAA CO-OPS, 2020c) and seven tidal constituents noted by Harris (1991) relevant for the US East Coast. Computations were performed in 1-year increments (3-year increments if greater than one month of data were missing within a year). Annual computations minimize timing errors that can lead to the leakage of tidal energy into the non-tidal residual (Merrifield et al., 2013). It also essentially removes the SLR trend and minimizes inherent constituent biases when computed over long time periods, which could result from changing physiographical environmental conditions (Ross et al., 2017) or from changing seasonal weather patterns that strongly influence the Sa (solar annual) and SSa (solar semi-annual) constituents (NOAA CO-OPS, 2007). More details on the computation of skew surge can be found in Callahan et al. (2021).

To help achieve stationarity and independence of data samples required by EVA, two further processes were performed on each gauge's time series. First, the mean and standard deviation of skew surge (as well as maximum TWL for comparison) at each gauge were computed and used to detrend the data about the 1980-2019 mean (Table 2). Second, skew surges were separated temporally by 30 hours. If multiple peaks above a selected water level threshold were within 30 hours of each other, they were treated as one event and only the maximum value was chosen, ensuring at least two high tides between each extreme skew surge.

2.3 Block Maxima/GEVr Approach

The BM approach of modeling extreme values is to select the maximum value within equal, independent blocks of time over the study period, which are usually fit to the GEV distribution. One-year blocks are commonly chosen (as in the current study) since a common ultimate goal is to estimate water levels of multiyear-based return periods for long-term planning purposes. Using the BM approach in this traditional way results in 40 data points over the years 1980 – 2019. The GEV distribution actually represents the combined generalized form of the Fréchet, Weibull, and Gumbel distributions, which have cumulative distribution functions (CDF) defined by Eq 2.1.

$$F(x|\mu,\sigma,\xi) = \Pr(X > x) = \begin{cases} \exp\left[-\left(1+\xi\left(\frac{x-\mu}{\sigma}\right)\right)^{-1/\xi}\right], & \xi \neq 0, \\ \exp\left[-\exp\left(-\left(\frac{x-\mu}{\sigma_\mu}\right)\right)\right], & \xi = 0, \end{cases} \tag{2.1}$$

where the quantity $1+\xi(x-\mu)/\sigma = \max(1+\xi(x-\mu)/\sigma, 0)$, with location parameter μ, scale parameter σ > 0, and shape parameter ξ. The shape parameter controls the shape of the tail. The second line of Eq 1 (ξ = 0) represents the Gumbel distribution and is found by taking the limit as ξ → 0. When ξ > 0 (Frechet), the tail is thicker than the Gumbel (i.e., "heavy-tailed") with no upper bound, whereas for ξ < 0 (Weibull), the distribution has a hard upper limit at μ - σ/ξ. Coles (2001) provides a detailed description of the BM/GEV approach.

A drawback of this approach is the limited number of data points (i.e., one per year) used to fit the model. Therefore, this method was generalized to include more than one value for each independent block of time by Weissman (1978) and later justified for use in hydrological studies, including modeling sea level extremes, by Tawn (1988). This extension of the BM approach allows for the use of the r-largest order statistics per year, permitted that r << total number of events per year. The key distinction of fitting data to the GEVr distribution, as opposed to the GEV distribution, is the choice of r. At r = 1, the GEV and GEVr are identical distributions. Since r is not a specific parameter in the GEVr probability density function, it cannot be estimate in the same way as μ, ξ, or σ.

Several orders of r were tested from 1 to 20 events per year. For each r, model parameters were estimated, and a series of hypothesis tests run. The upper limit choice of 20 was subjective but reasonable, as it would increase the number of data points significantly (20 * 40 yrs = 880, approximately 3% of all tidal peaks over 1980 – 2019) while keeping r << 730, the maximum number of twice-daily skew surge events per year. Ideally, r should be large enough to include

enough points to improve the robustness of the model but not large enough to introduce bias from the parent distribution and contaminating the EVD model fit.

A set of rules were developed by G'Sell et al. (2016) and furthered by Bader et al. (2017) to automate the selection of an optimum value of r. These rules are based on the sequential hypothesis tests for each r using the ForwardStop score and unadjusted p-value generated from parametric bootstrap and entropy difference tests. The ForwardStop score is an adjusted p-value to control for the incremental false discovery rate, similar to a weighted mean of p-values of all tests on previous r values (Bader et al., 2017). The over-riding principal here is to start with a minimum number of data points and slowly increase the sample size until the data points do not satisfactorily fit the GEVr distribution. Following guidance provided in Bader et al. (2017), the following procedure was adopted to identify the optimum r.

1. Start with r = 1 and note the ForwardStop score from the parametric bootstrap test. Incrementally increase r by 1 until the ForwardStop score fails hypothesis test at the $\alpha = 0.05$ level. If a failure occurs, that r is rejected and select the r just prior to the failed test.
2. If no r values are rejected after traversing all 20, use the ForwardStop score from the entropy difference test and repeat Step 1.
3. If no r values were rejected following Step 2, then repeat Steps 1-2 using the unadjusted p-values computed for each r instead of the ForwardStop score.
4. If no r values were rejected following Step 3, increase α to 0.10 and repeat Steps 1-3.

Using these guidelines, an optimum r was selected for each gauge. The Goodness-of-Fit (GoF) was then tested between the Gumbel distribution ($\xi = 0$) fit and the Fréchet/Weibull distribution ($\xi \neq 0$) fit using the negative log-likelihood ratio test (ratio must be greater than 0.95) and Akaike Information Criterion (AIC) test (the difference in AIC score between sequential tests must be > 2, described in Burnham and Anderson (2004)). Maximum likelihood estimation (MLE) was used for all GEVr model fits. Temporal declustering of skew surge peaks was performed on an annual basis in order for each of the r-largest orders per year to be an independent event.

2.4 Points-Over-Threshold/GP Approach

In contrast to the BM approach, the POT approach is a more natural way of statistically modeling the upper tail of a parent distribution. The entire study period is treated as a single block and the EVD includes only observations over a certain threshold value (i.e., exceedances) regardless of time the event occurred. The threshold is derived from a suitably high quantile level (e.g., 97% quantile is commonly used). Exceedances are then fit to the Generalized Pareto (GP) distribution. Like the GEV, the GP distribution represents a family of three distributions, differentiated by the model shape parameter, the CDFs of which are in Eq 2.2.

$$F\left(x|\mu,\sigma_\mu,\zeta\right) = Pr(X < x \mid X > \mu) = \begin{cases} 1 - \left[1 + \xi\left(\dfrac{x-\mu}{\sigma_\mu}\right)\right]^{-1/\xi}, & \xi \neq 0, \\ 1 - exp\left[-\left(\dfrac{x-\mu}{\sigma_\mu}\right)\right], & \xi = 0, \end{cases} \tag{2.2}$$

where the quantity inside the brackets $[y] = \max([y], 0)$, suitably high threshold μ, threshold-dependent scale parameter $\sigma_\mu > 0$, and shape parameter ξ. The condition is that all values of x must be larger or equal to the threshold μ. Behavior of the parameters is similar to that in the GEV. The shape parameter controls the shape of the tail. The second line of Eq. 2 is found by taking the limit as $\xi \rightarrow 0$, resulting in the Exponential distribution. A heavy tail occurs when $\xi > 0$ (Pareto distribution) with no upper bound, whereas a thinner tail and a fixed upper bound occurs when $\xi < 0$ (Beta distribution). Coles (2001) provides a detailed description of the POT/GP approach.

Threshold quantiles were tested from 90 – 99.5% exceedance probabilities in increments of 0.5% (from 1 – 20 thresholds), resulting in the maximum number of possible skew surge peaks used to model GP to be approximately 2,920 (90%) to 146 (99.5%). A threshold should be chosen to include enough upper tail exceedances that will improve the robustness of the model but not too many exceedances such that the lower values introduce bias from the parent distribution. Scarrott and MacDonald (2012) reviewed various methods on selecting the optimum threshold, including numerical tests and graphical diagnostics, such as Quantile-Quantile and Mean Residual Life plots. Many of these selection methods are subjective, time-consuming when investigating many sites, and often result in multiple acceptable answers. Diagnostic plots were used in the current study (Supplement Figures 1 – 24), however, to better compare results with BM/GEVr approach, a similar standardized methodology was employed for selecting an optimum threshold.

The rules developed by G'Sell et al. (2016) and Bader et al. (2017) were applied to automate the selection of the optimum threshold of the POT/GP approach in Bader et al. (2018). Unadjusted p-values from Anderson-Darling test was chosen in Bader et al. (2018) for threshold sequential hypothesis testing after a comparison among several other GoF tests. Although Bader et al. (2018) recommends using ForwardStop score, based on skew surge data in the current study, ForwardStop rejects very few thresholds and the unadjusted p-values performed well in Bader et al. (2018) tests. Using the same over-riding principal here as with the BM/GEVr approach, start with the least number of data points and slowly increase the sample size until the data points do not satisfactorily fit the GP model. This is essentially working backwards, from the highest to lowest threshold, noted as the RawDown approach in Bader et al. (2018). A RawUp approach, working upwards from the minimum threshold (i..e, most data points) until a hypothesis test was accepted, was also described in Bader et al. (2018) but carries a higher chance for contaminating the EVD than the RawDown approach. Ultimately, the following rules were adopted to identify the optimum threshold.

1. Start with highest threshold percentage (99.5%) and note the unadjusted p-value from the Anderson-Darling test. Incrementally decrease the threshold percentage by 0.5% until the GP model fit fails hypothesis test at $\alpha = 0.05$ level. If a failure occurs, that threshold is rejected and select the threshold just prior to the failed test.
2. If the highest threshold (99.5%) is rejected on the first test but the second (99.0%) is not rejected, then skip the highest threshold and continue working downward until next rejection occurs. This allows for the opportunity to include more exceedances in the model and assumes the rejection occurred by chance.
3. If no thresholds were rejected following Step 2, increase α to 0.10 and repeat Steps 1-2.

Using these guidelines, an optimum threshold was selected for each gauge. Temporal declustering was performed separately for each threshold on all exceedances over the entire study period at once. Declustering therefore significantly reduced the actual number of skew surge events used in fitting the GP model by approximately 30 – 70%. Maximum likelihood estimation (MLE) was used for all GP model fits.

2.5 Skew Surge Return Levels

Lastly, return level (RL) skew surges were estimated for 1.1, 3, 5, 10, 25, 50, and 100-year return periods for each EVA modeling approach. A RL represents a threshold that the probability of exceedance in any one year is the inverse of the return period. For example, 100-yr RL has a 1.0% (0.01) probability of being exceeded in any one year. Since the 1-yr RL is undefined within the BM/GEVr approach, 1.1-yr was used instead for comparison.

Although probability quantiles can be easily extracted from the GP theoretical distribution using the fitted parameters, they cannot be viewed as annual probabilities of return levels, such as can be done using the BM/GEVr approach. Therefore, an estimate of the probability of a skew surge exceeding a selected threshold in a year on average must be included in RL calculations using the POT/GP approach. This is found by dividing the total number of declustered skew surge events above the selected threshold by the total number of years (40).

A qualitative review was performed on the estimated model parameters and return levels, with their 95% standard errors (SE) modeled using the selected optimum r (BM/GEVr) and threshold (POT/GP). Differences between the EVA modeling approaches and spatial variations were noted.

The harmonic analysis and tidal data processing work was done using the U-Tide package (Codiga, 2011) and standard modules in the Matlab programming environment. Temporal declustering was performed using the *POT* package (Ribatet and Dutang, 2019) and the EVA model fitting and RL extraction were performed using the *eva* package (Bader, 2020), both of the R statistical computing software environment.

3 Results

3.1 Skew Surge

Basic statistics of skew surge and TWL over the entire study period to get a sense of the parent distributions before detrending and EVA. Mean skew surges are consistent and very close to zero across all tide gauges whereas TWL shows much larger geographic variation (Table 2). Although differences are minor, largest skew surges (0.2 m) are at PHL and the open ocean gauges at ATL and WAC. TWL is consistently higher in the Delaware Bay than the Chesapeake Bay. Within each bay, the Delaware Bay upper regions have higher max TWL than the lower regions, whereas this pattern is reversed in the Chesapeake Bay. Spatial pattern of max TWL aligns with the Mean Higher-High Water (MHHW) and Great Diurnal Range (GT) tidal datums (Figure 3), which do not align with the spatial pattern of skew surge. Standard deviations of skew surge show slightly more geographic variation (ranging 0.14 – 0.19 m) with a similar spatial pattern to the max TWL and Mean Sea Level (MSL) tidal datum. Largest deviations are in the upper bays and lowest in the central Chesapeake Bay.

Table 2. *Mean and standard deviation of detrended maximum total water level (TWL) and skew surge for all tidal peaks observed during 1980 – 2019. Mean Seal Level (MSL), Mean Higher-High Water (MHHW), and Great Diurnal Range (GT) tidal datums defined by NOAA for the current National Tidal Datum Epoch (NTDE) 1983-2001. All water levels referenced to NAVD88 meters.*

Station	Max TWL		Skew Surge		Tidal Datum		
	Mean	SD	Mean	SD	MHHW	MSL	GT
Philadelphia	1.01	0.27	0.02	0.19	1.09	0.12	2.04
Reedy Point	0.81	0.25	-0.01	0.17	0.99	-0.02	1.78
Lewes	0.52	0.26	0.01	0.16	0.62	-0.12	1.42
Cape May	0.65	0.26	0.01	0.15	0.74	-0.14	1.66
Atlantic City	0.51	0.26	0.02	0.16	0.61	-0.12	1.40
Baltimore	0.19	0.24	0.00	0.18	0.25	-0.01	0.51
Annapolis	0.16	0.22	0.00	0.17	0.20	-0.02	0.44
Cambridge	0.25	0.20	0.00	0.16	0.29	-0.03	0.62
Lewisetta	0.21	0.20	0.00	0.14	0.21	-0.02	0.46
Kiptopeke	0.27	0.20	0.01	0.14	0.32	-0.15	0.90
Sewells Point	0.33	0.21	0.01	0.15	0.35	-0.08	0.84
Wachapreague	0.50	0.24	0.02	0.15	0.57	-0.11	1.36

None of the gauges showed statistically significant trends in skew surge except for PHL, which showed a slight negative trend of approximately -0.3 mm/yr. For comparison, all gauges showed statistically significant trends in max TWL consistent with local SLR rates (further analysis was not performed on max TWL.)

As an example of the parent vs upper tail distributions, Figure 2 (left panel) shows the histogram of all detrended skew surges for the LEW tide gauge over the study time period (N = 28,231) with a zoomed-in view of the upper tail (right panel). The Normal distribution fit significantly underestimates the empirical data in much of the upper tail, emphasizing the importance of modeling extremes of skew surge separately from the parent distribution.

3.2 Model Parameter Selection

Figure 3 shows an example of the GEVr sequential hypothesis testing for the LEW gauge. No rejections occurred (below $\alpha = 0.05$) using ForwardStop score from either the parametric bootstrap or entropy difference procedures. Staring from r = 1 and sequentially comparing the unadjusted p-values, the first rejection occurs at r = 15, resulting in the optimum r = 14. Testing for the optimum threshold in the POT/GP approach worked in the same way, albeit starting on the right side of the unadjusted p-values plot and working downward until a rejection occurs following guidance in Section 2.4.

Table 3 and Figure 4 show resultant model parameters estimated after selecting the optimum r in the BM/GEVr approach at each gauge. The number of skew surge events per year that were fit to the GEVr distribution, ranges from N = 120 (r = 3 at CAP, ANN, SEW) to N = 560 (r = 14 at LEW). Both the location and scale parameters have small, consistent SE relative to their magnitude across all sites. The shape parameter is the most uncertain of all the parameters, although SE is relatively consistent across all sites. Uncertainty is inversely related to the total number of skew surge events

ultimately used in the EVA after declustering; the lower the number of events, the smaller the SE. Shape parameter is positive at all sites except at WAC where it is slightly negative. Based on the negative log-likelihood ratio and AIC difference tests, none of sites favor the use of the GEVr Gumbel ($\xi = 0$) distribution over the GEVr Fréchet/Weibull ($\xi \neq 0$) distribution.

Table 3. *Results from GEVr distribution model fit of extreme skew surges for tide gauges in the Mid-Atlantic region. R is the number of largest maxima per year included in the analysis. Npks is the number of skew surge events after 30-hr temporal declustering and is equal to r multiplied by the number of years of data. Location, scale, and shape are model parameters fit using maximum likelihood estimation (MLE) with 95% standard error in parentheses.*

Station	r	Npks	Location	Scale	Shape
Philadelphia	7	280	0.636 (0.017)	0.134 (0.012)	0.082 (0.058)
Reedy Point	11	440	0.547 (0.015)	0.117 (0.010)	0.039 (0.046)
Lewes	14	560	0.699 (0.023)	0.180 (0.017)	0.102 (0.044)
Cape May	3	120	0.602 (0.018)	0.128 (0.013)	0.121 (0.083)
Atlantic City	6	240	0.700 (0.022)	0.166 (0.014)	0.034 (0.059)
Baltimore	12	480	0.611 (0.016)	0.128 (0.012)	0.113 (0.047)
Annapolis	3	120	0.566 (0.016)	0.112 (0.012)	0.165 (0.085)
Cambridge	11	440	0.561 (0.014)	0.111 (0.010)	0.062 (0.047)
Lewisetta	10	400	0.507 (0.013)	0.106 (0.009)	0.064 (0.049)
Kiptopeke	4	160	0.566 (0.019)	0.140 (0.013)	0.075 (0.071)
Sewells Point	3	120	0.671 (0.025)	0.178 (0.017)	0.093 (0.081)
Wachapreague	11	418	0.691 (0.020)	0.156 (0.012)	-0.057 (0.043)

Similarly, Table 4 and Figure 3 summarize the results after selecting the optimum threshold using the POT/GP approach at each gauge. Threshold percentages range from 94.5% (ATL, N = 732) to 99.0% (LEW, ANN, KIP, and SEW, N = 160, 194, 139, and 142, respectively.) Gauges that have the same optimum threshold still result in different total number of skew surge events due to temporal declustering. Scale parameter SE is low while the shape parameter SE is relatively high across all sites. Shape parameter is positive at all sites except at KIP where it is slightly negative. Spatial patterns and relative uncertainties of both the scale and shape parameter estimates are generally similar between the two approaches.

Supplemental Figures 1 – 12 (BM/GEVr) and 13 – 24 (POT/GP) show diagnostic plots of the model fit using the optimally selected r and threshold values at each tide gauge. Included are probability-probability (PP) and quantile-quantile (QQ) plots of the modeled vs empirical data, and histograms overlaid with model fit PDF curve. The PP plots and histograms show good agreement between the model and observations. For most gauges, the QQ plots show a few outliers with the observed skew surge levels higher than modeled quantile estimates. The LEW gauge did not show this behavior but rather at the largest values, the modeled quantiles were larger than the observed data.

Table 4. *Results from GP distribution model fit of extreme skew surges for tide gauges in the Mid-Atlantic region. Npks is the number of skew surge events above threshold percent quantile after 30-hr temporal declustering. Scale and shape are model parameters fit using maximum likelihood estimation (MLE) with 95% standard error in parentheses.*

Station	Threshold	Npks	Scale	Shape
Philadelphia	94.50	744	0.124 (0.006)	0.020 (0.037)
Reedy Point	96.50	497	0.108 (0.007)	0.034 (0.046)
Lewes	99.00	160	0.166 (0.019)	0.032 (0.082)
Cape May	93.50	784	0.129 (0.007)	0.004 (0.036)
Atlantic City	94.00	732	0.146 (0.008)	0.034 (0.038)
Baltimore	98.50	301	0.087 (0.008)	0.187 (0.068)
Annapolis	99.00	194	0.097 (0.010)	0.123 (0.081)
Cambridge	96.00	641	0.104 (0.006)	0.016 (0.040)
Lewisetta	98.50	211	0.094 (0.009)	0.071 (0.074)
Kiptopeke	99.00	139	0.144 (0.017)	-0.015 (0.084)
Sewells Point	99.00	142	0.174 (0.021)	0.044 (0.088)
Wachapreague	98.00	224	0.151 (0.015)	0.052 (0.070)

3.3 Skew Surge Return Levels

Skew surge return levels for 1.1, 3, 5, 10, 25, 50, and 100-year return periods with 90% confidence intervals (i.e., uncertainty) are shown in Table 5 for BM/GEVr and Table 6 for POT/GP. For the sake of brevity and ease of comparison, only the mean values are plotted in Figure 5. Note the more traditional continuous RL curves with confidence intervals are included in Supplemental Figures 25 – 26, and additionally plotted with empirical data in panel 4 of Supplemental Figures 1 –24. RLs increase in a consistent manner with longer return periods at all sites under both modeling approaches. For BM/GEVr, 100-yr RLs range from 1.07 m (LWS) to 1.79 m (LEW) with generally largest values starting in the lower bay regions, decreasing to a minimum in the central regions, then increasing toward the upper regions. This pattern is similar across all RLs. LEW and SEW have the largest RLs for most return periods, except for the 1.1-yr return period, where the maximum RL is at ATL (although several other sites are very close). Longer return periods demonstrate more spatial variation in RLs. Using POT/GP, 100-yr RLs range from 1.08 m (LWS) to 1.56 m (LEW), with approximately the same spatial pattern as with BM/GEVr.

There are few differences in RLs between approaches (Table 7; Figure 6). The most noticeable is that the 1.1-yr RLs using BM/GEVr (0.45 – 0.56 m) are significantly lower than using POT/GP (0.52 – 0.72 m) at all sites. At the other extreme, BM/GEVr 100-yr RLs are generally higher, mostly in the upper bay regions, with LEW (0.19 m) and CAP (0.17 m) showing the largest positive differences between methods. BAL (-0.15 m) and WAC (-0.20 m) are exceptions, with higher 100-yr RLs using POT/GP. Most return periods between 3-yr and 50-yr show small differences in RLs across most gauges.

Table 5. *Estimated skew surge return levels for 1.1, 3, 5, 10, 25, 50, and 100-yr return periods modeled using the BM/GEVr approach for tide gauges in the Mid-Atlantic region. 90% confidence intervals in parentheses. All data referenced to NAVD88 meters.*

Station	1.1-yr	3-yr	5-yr	10-yr	25-yr	50-yr	100-yr
PHL	0.52 (0.04)	0.76 (0.12)	0.85 (0.16)	0.97 (0.25)	1.13 (0.40)	1.25 (0.55)	1.38 (0.74)
RDY	0.45 (0.04)	0.65 (0.09)	0.73 (0.12)	0.82 (0.18)	0.95 (0.27)	1.04 (0.35)	1.14 (0.45)
LEW	0.55 (0.06)	0.87 (0.16)	0.99 (0.23)	1.16 (0.35)	1.38 (0.55)	1.56 (0.75)	1.76 (0.99)
CAP	0.50 (0.05)	0.72 (0.12)	0.81 (0.18)	0.93 (0.30)	1.10 (0.54)	1.24 (0.81)	1.39 (0.99)
ATL	0.56 (0.06)	0.85 (0.14)	0.96 (0.20)	1.09 (0.30)	1.26 (0.48)	1.39 (0.66)	1.53 (0.88)
BAL	0.50 (0.04)	0.73 (0.11)	0.82 (0.15)	0.94 (0.23)	1.10 (0.36)	1.24 (0.49)	1.38 (0.65)
ANN	0.47 (0.04)	0.67 (0.11)	0.76 (0.16)	0.87 (0.26)	1.04 (0.47)	1.18 (0.64)	1.34 (0.72)
CAM	0.47 (0.04)	0.66 (0.09)	0.74 (0.13)	0.83 (0.20)	0.95 (0.31)	1.05 (0.41)	1.15 (0.54)
LWS	0.42 (0.03)	0.61 (0.09)	0.67 (0.12)	0.76 (0.18)	0.88 (0.27)	0.98 (0.37)	1.07 (0.48)
KIP	0.45 (0.05)	0.70 (0.13)	0.79 (0.19)	0.91 (0.31)	1.07 (0.55)	1.20 (0.79)	1.33 (1.11)
SEW	0.52 (0.07)	0.84 (0.16)	0.96 (0.24)	1.12 (0.39)	1.33 (0.70)	1.51 (1.02)	1.69 (1.43)
WAC	0.55 (0.06)	0.83 (0.11)	0.92 (0.14)	1.02 (0.19)	1.15 (0.26)	1.24 (0.32)	1.32 (0.39)

Table 6. *Estimated skew surge return levels for 1.1, 3, 5, 10, 25, 50, and 100-yr return periods modeled using the POT/GP approach for tide gauges in the Mid-Atlantic region. 90% confidence intervals in parentheses. All data referenced to NAVD88 meters.*

Station	1.1-yr	3-yr	5-yr	10-yr	25-yr	50-yr	100-yr
PHL	0.66 (0.06)	0.79 (0.11)	0.86 (0.14)	0.95 (0.19)	1.08 (0.27)	1.18 (0.35)	1.28 (0.44)
RDY	0.56 (0.06)	0.68 (0.10)	0.74 (0.27)	0.83 (0.18)	0.95 (0.26)	1.04 (0.34)	1.14 (0.43)
LEW	0.72 (0.08)	0.90 (0.16)	0.99 (0.22)	1.12 (0.35)	1.29 (0.61)	1.43 (0.88)	1.56 (1.23)
CAP	0.62 (0.06)	0.75 (0.11)	0.82 (0.14)	0.91 (0.19)	1.03 (0.27)	1.12 (0.34)	1.21 (0.42)
ATL	0.71 (0.08)	0.88 (0.14)	0.97 (0.18)	1.08 (0.25)	1.25 (0.36)	1.37 (0.46)	1.50 (0.58)
BAL	0.61 (0.06)	0.76 (0.13)	0.84 (0.19)	0.97 (0.30)	1.16 (0.52)	1.33 (0.77)	1.53 (1.09)
ANN	0.58 (0.06)	0.71 (0.11)	0.78 (0.16)	0.88 (0.25)	1.03 (0.42)	1.16 (0.60)	1.30 (0.84)
CAM	0.58 (0.05)	0.69 (0.09)	0.74 (0.11)	0.82 (0.15)	0.93 (0.21)	1.01 (0.27)	1.09 (0.34)
LWS	0.52 (0.05)	0.63 (0.10)	0.69 (0.13)	0.77 (0.20)	0.89 (0.32)	0.98 (0.44)	1.08 (0.60)
KIP	0.59 (0.07)	0.73 (0.12)	0.80 (0.16)	0.89 (0.25)	1.02 (0.41)	1.11 (0.58)	1.20 (0.80)
SEW	0.69 (0.09)	0.88 (0.16)	0.98 (0.23)	1.12 (0.35)	1.31 (0.60)	1.46 (0.85)	1.61 (1.17)
WAC	0.68 (0.08)	0.85 (0.22)	0.94 (0.36)	1.07 (0.32)	1.25 (0.51)	1.38 (0.77)	1.53 (1.25)

Uncertainty also increases with longer return periods under both approaches, as expected. At 1.1-yr return period the uncertainties are less than 0.10 m, and range 0.18 – 0.39 m at 10-yr, and 0.30 – 1.43 m at 100-yr. Sites in the Chesapeake Bay, under both approaches, exhibit spatial variation in uncertainty similar to that of the mean RL estimates, with the largest uncertainties in the lower bay regions, smallest in the central regions, and increasing in the upper regions. WAC is an exception to this with small uncertainty under BM/GEVr. Sites in the Delaware Bay also show this same pattern in uncertainty with BM/GEVr but not POT/GP, under which CAP and ATL (sites in the lower bay region) show small uncertainties.

Generally, uncertainties under both approaches are very similar to each other at shorter return periods. At longer return periods in the Delaware Bay, uncertainties are smaller using POT/GP for most sites. At longer return periods in the Chesapeake Bay, generalization is more difficult; BAL (-0.44 m at 100-yr) and WAC (-0.87 m at 100-yr) have significantly smaller uncertainties using BM/GEVr while many other sites have smaller uncertainties using POT/GP.

Table 7. *Difference in estimated skew surges and 90% confidence intervals (in parentheses) for 1.1, 3, 5, 10, 25, and 100-yr return periods modeled from GEVr and GP distribution for tide gauges in the Mid-Atlantic region. Negative values mean GP estimates are greater than GEVr estimates. All data referenced to NAVD88 meters.*

Station	1.1-yr	3-yr	5-yr	10-yr	25-yr	50-yr	100-yr
PHL	-0.13 (-0.02)	-0.03 (0.01)	-0.01 (0.02)	0.01 (0.06)	0.05 (0.13)	0.07 (0.20)	0.11 (0.30)
RDY	-0.11 (-0.02)	-0.03 (-0.01)	-0.02 (-0.15)	-0.01 (0.00)	-0.01 (0.00)	0 (0.01)	0 (0.02)
LEW	-0.17 (-0.03)	-0.03 (0.01)	0 (0.01)	0.04 (0.00)	0.09 (-0.06)	0.14 (-0.13)	0.19 (-0.23)
CAP	-0.12 (-0.02)	-0.03 (0.01)	-0.01 (0.04)	0.02 (0.11)	0.07 (0.27)	0.12 (0.47)	0.17 (0.57)
ATL	-0.16 (-0.02)	-0.03 (0.00)	-0.01 (0.02)	0 (0.05)	0.01 (0.12)	0.02 (0.20)	0.03 (0.30)
BAL	-0.11 (-0.02)	-0.02 (-0.03)	-0.02 (-0.04)	-0.03 (-0.08)	-0.06 (-0.17)	-0.10 (-0.28)	-0.15 (-0.44)
ANN	-0.11 (-0.02)	-0.03 (-0.01)	-0.02 (0.00)	-0.01 (0.02)	0 (0.05)	0.02 (0.05)	0.04 (-0.12)
CAM	-0.11 (-0.02)	-0.02 (0.01)	-0.01 (0.02)	0.01 (0.05)	0.03 (0.09)	0.05 (0.14)	0.07 (0.21)
LWS	-0.10 (-0.02)	-0.02 (-0.01)	-0.01 (-0.01)	-0.01 (-0.02)	-0.01 (-0.04)	-0.01 (-0.07)	-0.01 (-0.12)
KIP	-0.14 (-0.02)	-0.03 (0.01)	-0.01 (0.03)	0.01 (0.06)	0.05 (0.13)	0.09 (0.21)	0.13 (0.31)
SEW	-0.17 (-0.02)	-0.04 (0.00)	-0.02 (0.01)	0 (0.04)	0.03 (0.10)	0.05 (0.18)	0.08 (0.26)
WAC	-0.13 (-0.02)	-0.03 (-0.11)	-0.03 (-0.22)	-0.05 (-0.13)	-0.10 (-0.26)	-0.15 (-0.45)	-0.20 (-0.87)

4 Discussion

The primary focus of the current study is to estimate return levels of skew surge for up to 100-yr return periods and investigate the magnitude and geographic variation within the Delaware and Chesapeake Bays to aid in long-term planning of the many coastal communities and critical ecosystems along its shores. Extreme events are important because of their potential for severe damage and threat to public health. And skew surge is arguably one of the best and simplest measures of the meteorological (i.e., non-tidal, non-SLR) drivers of coastal flooding although its use in literature has only recently gained attention.

This work was done strictly through empirical data (rather than using simulated or scenario-based surge projections) recorded over the past 40 years and statistically analyzed through stationary EVA on detrended skew surges. Observational data showed minimal trends over this time period, hence results from this study should not be appreciably different than non-stationary EVA (i.e., allowing for temporally varying or multivariable dependent location and scale parameters.) Due to the approximate independence of skew surge to SLR, and likely minor influences of tide-surge interactions at our sites, return levels can reasonably be incorporated into future SLR scenarios, or other related trends in flood frequency, high tides, and tidal ranges. Values for skew surge estimates in this work are relative to the 1980 – 2019 mean, referenced to NAVD88 vertical datum, which

should be considered when assessing future flooding potential, although the mean values at all sites are within a few centimeters of zero (Table 2).

Largest return levels across most return periods occur within the bay boundaries in the lower regions, and not in the upper regions of the Delaware Bay and ocean coast sites that typically show higher surges, TWLs, and larger tidal ranges. Specially, LEW and SEW gauges, both located on the southwest side of the mouth of each bay, consistently show the largest RLs throughout the region. One explanation is that many large coastal flood events are associated with ETCs, many of those as traditional nor'easters. The low-pressure centers off the coast bring strong northeast winds, which drives enhanced surges into the bays through Ekman transport but also direct winds piling up water on the southwest sides of the lower bays. This would be most effective in the lower Delaware Bay, where the width of the Bay reaches 45 km. The upper Delaware Bay, although it experiences large tidal ranges and increased surges (due to conical shape of coastline and from the increased volume of water entering the bay from southeasterly to easterly winds), may not experience the worst impacts from the most extreme storm events and may actually see decreases in surges from northerly winds that also occur during nor'easters. The upper Chesapeake Bay does not exhibit the same high TWL, MHHW, or surges as in the upper Delaware Bay (primarily due to the overall size, shape, and depth of the Chesapeake Bay), however, extreme skew surge RLs in both upper regions are comparable to each other. This supports results in Callahan et al., 2021, which found the upper bays were highly correlated with each other from TC-caused skew surges, even more so than with their respective lower bay regions. TCs can account for close to 50% of the largest (top 10) coastal flooding events in the Mid-Atlantic, with smaller relative percentages over larger number of events (Booth et al., 2016; Callahan, preliminary research). In particular for the upper Chesapeake Bay, Hurricane Isabel in 2003 caused extreme coastal flooding compared to other events, serving as an outlier and directly increasing higher return period RLs and their uncertainties.

RLs tend to be at a minimum within each bay closer to the central regions, CAM and LWS in the Chesapeake and RDY in the Delaware Bays. These areas have the lowest mean skew surges throughout the region and typically do not experience the worst wind-driven impacts from coastal storms. Likewise, these areas also exhibit the smallest uncertainties throughout the region across many return periods.

A secondary focus of this study is to provide insight into the two most common approaches of stationary EVA applied to Mid-Atlantic skew surge. To that end, the GEVr distribution was combined with the BM approach (to address the small sample size of the traditional annual max BM/GEV approach) and a standardized method to selecting optimum r and threshold was incorporated. The use of GEVr increases the robustness of the model fit and puts the number of data points more comparable to the POT/GP approach, however there are some disadvantages of using a BM approach. Large surge events could be missed, for example, if an individual year has more major coastal flood events than the selected optimum r (i.e., false positives). At the other end, non-extreme surge events could be included, for example, if an individual year has less major coastal flood events than the selected optimum r, introducing bias from the parent distribution (i.e., false negatives). Use of the POT/GP approach circumvents these issues as it is irrespective of time, solely focused on the upper tail of the parent distribution. A potential trade-off is if the majority of extreme events occur towards either end of the study time period, direct interpretation of annual return levels from the mean number of events per year is more difficult. From review of the data used in the current study, clustering of major skew surge events occurring on either end of the time period was not present.

570 The choice of optimum r or threshold is a tricky problem to address. It is usually a subjective process,
571 including graphical and numerical diagnostic information, and choosing among multiple appropriate
572 candidates. The current study incorporates a standardized methodology of sequential hypothesis
573 texting that can be applied to all sites simultaneously while allowing for variable r/threshold selection
574 per site. Although stopping rules and goodness of for tests are still subjective within this
575 methodology, they are data-driven, based on statistical results from Bader et al. (2017) and Bader et
576 al. (2018). Choice of stopping rules influences the number of data points (r-largest orders or
577 threshold exceedances), and hence, directly influence the uncertainty in model parameters.
578 Uncertainty in RLs do not consistently show strong dependence on the number of peaks included in
579 the model fit. This potential relationship of RL uncertainty and optimum r/threshold should be
580 explored further in future work.

581 Determination of which approach is "best" for modeling extreme skew surge events in the Mid-
582 Atlantic is not a goal of the current study. Nevertheless, differences between the approaches are
583 highlighted and some general recommendations can be made. Overall, both approaches provide
584 similar results. Confidence in model parameters is good and consistent across all sites between both
585 approaches, with narrow confidence intervals for the location and scale parameters. Confidence is
586 less for shape parameter but is generally the same for both approaches. Not many differences in
587 magnitude of RLs exist, especially for 3-yr to 100-yr return periods, which helps justify comparisons
588 of extreme levels of surge among previous EVA studies in this region (at least for skew surge).

589 For the 1.1-yr return period, the POT/GP approach provides more consistent values in respect to
590 other return periods across both bays. This is likely due to the effects of estimating RLs from the
591 GEVr distribution close to 1-yr. For the Delaware Bay at longer return periods, the POT/GP also
592 seems to perform well (lower uncertainty) at most sites and therefore could be used at all return
593 periods from 1 to 100 years. Recommendations are more mixed for the Chesapeake Bay for return
594 periods at 3-yr and above. Results at ANN and LWS are nearly identical for both approaches. For
595 KIP and SEW, sites in the lower Chesapeake Bay, lower uncertainties and slightly lower RLs tend
596 toward the POT/GP approach. Conversely, BAL (upper region) and WAC (ocean coast) tend toward
597 the use of the BM/GEVr approach.

598 Changes in storm frequency or intensity ("storminess"), either observed or projected due to climate
599 change, were not addressed in this study. As stated above, skew surge is closely related to the
600 meteorological characteristics of the storm/wind event driving the flooding and relatively
601 independent of SLR. Long period trends in skew surge can also be influenced by oscillations and
602 trends in oceanic-atmospheric circulation patterns, commonly measured through North Atlantic
603 Oscillation, Pacific-North American oscillation, Atlantic Meridional Overturning Circulation, El
604 Nino/Southern Oscillation, and other large-scale synoptic phenomena (Ezer et al., 2013; Sweet et al.,
605 2014; Hamlington et al., 2015; Wahl and Chambers, 2015; Rashid et al., 2017; Kopp et al., 2019;
606 Little et al., 2019). These oscillations could be included as covariates in non-stationary EVA of skew
607 surges or integrated as joint probabilities of their own extreme RLs and warrant further investigation.
608 The 40-yr time period of this study is long enough to capture several oscillations of many of these
609 teleconnections, and RLs can be viewed as based on relative aggregate conditions. However, the
610 probability of occurrence of an extreme surge level in any one year is, at least partly, dependent upon
611 the prevailing synoptic conditions.

612 Other aspects of this study could have influenced extreme surge estimates. Most notably is the
613 length of the data record, as is usually the case in EVA. Forty years of data to estimate 100-yr RL is
614 not ideal. Comparing the results of a similar EVA on a select set of gauges with much longer records

615 could offer insight into the robustness of the current study statistical results. Additionally, the set of
616 44 constituents used in the HA computation of the predicted tide may not capture all the tidal
617 oscillations present at every site, thereby impacting the magnitude of skew surge (albeit these
618 changes likely would be minimal). The choice of 30 hrs was subjective and may not be optimum at
619 all sites to separate individual skew surge events, although it is rare for a single storm event to reach
620 extreme surge levels multiple times separated by two or more high tides.

621

Abbreviations Used in This Manuscript

NOAA Tide Gauge Locations – Philadelphia (PHL), Reedy Point (RDY), Lewes (LEW), Cape May (CAP), Atlantic City (ATL), Baltimore (BAL), Annapolis (ANN), Cambridge (CAM), Lewisetta (LWS), Kiptopeke (KIP), Sewells Point (SEW), Wachapreague (WAC)

BM – Block Maxima

ETC/TC - Extratropical Cyclone (also called mid-latitude cyclones)/Tropical Cyclone

EVA/EVD – Extreme Value Analysis/Extreme Value Distribution

GEV – Generalized Extreme Value distribution

GEVr – Generalized Extreme Value r-largest order distribution

GoF – Goodness-of-Fit test

GP – Generalized Pareto distribution

HA – Harmonic Analysis

MLE – Maximum Likelihood Estimation

MHHW - Mean Higher-High Water tidal datum

MSL - Mean Sea Level tidal datum

NAVD88 - North American Vertical Datum of 1988

NTDE - National Tidal Datum Epoch

NTR - Non-tidal residual

NWLON - NOAA NOS National Water Level Observation Network

PORTS - NOAA National Ocean Service Physical Oceanographic Real-Time System

POT – Points Over Threshold

RL – Return Level

SLR – Sea-Level Rise

SST - Sea Surface Temperature

SE – Standard Error

TWL - Total Water Level

References

Bader, B., and Yan, J. (2020). eva: Extreme Value Analysis with Goodness-of-Fit Testing.

Bader, Brian, Yan, Jun, and Zhang, Xuebin, 2017. Automated selection of r for the r largest order statistics approach with adjustment for sequential testing. *Statistics and Computing*, 27, 1435-1451, DOI:10.1007/s11222-016-9697-3

Bader, Brian, Yan, Jun, and Zhang, Xuebin (2018). Automated Threshold Selection for Extreme Value Analysis via Ordered Goodness-of-Fit Tests with Adjustments for False Discovery Rate. *The Annals of Applied Statistics*. 12, 1, 310-329, DOI:10.1214/17-AOAS1092

Batstone, C., Lawless, M., Tawn, J., Horsburgh, K., Blackman, D., McMillan, A., D. Worth, Laeger, S., and Hunt, T. (2013). A UK best-practice approach for extreme sea-level analysis along complex topographic coastlines. *Ocean Engineering*, 71, 28–39. DOI:10.1016/j.oceaneng.2013.02.003.

Bernier, N. B. and Thompson, K. R. (2007). Tide-surge interaction off the east coast of Canada and northeastern United States. *Journal of Geophysical Research*, 112, C06008. DOI:10.1029/2006JC003793

Bernier, N.B. and Thompson, K.R. (2006). Predicting the frequency of storm surges and extreme sea levels in the northwest Atlantic. *Journal of Geophysical Research: Oceans*, 111:10, DOI:10.1029/2005JC003168

Blake, E. S. and Gibney, E. J. (2011). The deadliest, costliest, and most intense United States tropical cyclones from 1851to 2010 (and other frequently requested hurricane facts). NOAA Technical Memorandum NWS NHC-6. 49 pp.

Boesch, D. F., Boicourt, W. C., Cullather, R. I., Ezer, T., Galloway, G. E., Jr., Johnson, Z. P., Kilbourne, K. H., Kirwan, M. L., Kopp, R. E., Land, S., Li, M., Nardin, W., Sommerfield, C. K., Sweet, W. V. (2018). Sea-level Rise: Projections for Maryland 2018, 27 pp. University of Maryland Center for Environmental Science, Cambridge, MD.

Boon, John D., Mitchell, M., Loftis, J. D., and Malmquist, D. L. (2018). Anthropogenic Sea Level Change: A History of Recent Trends Observed in the U.S. East, Gulf and West Coast Regions, Special Report No. 467 in Applied Marine Science and Ocean Engineering, prepared by Virginia Institute of Marine Science, VA, 76 pp.

Booth, J. F., Rider, H. E., and Kushnir, Y. (2016). Comparing hurricane and extratropical storm surge for the Mid-Atlantic and Northeast Coast of the United States for 1979–2013. *Environmental Research Letters*, 11:9, 094004. DOI:10.1088/1748-9326/11/9/094004

Burnham, Kenneth P., and Anderson, David R. (2004). Multimodel Inference: Understanding AIC and BIC in Model Selection. *Sociological Methods and Research*. DOI:10.1177/0049124104268644

Calafat, Francisco M., and Marcos, Marta (2020). Probabilistic reanalysis of storm surge extremes in Europe. *PNAS*, 117, 4, 1877-1883. DOI:10.1073/pnas.1913049117

683 Callahan, John A., Daniel J. Leathers, Christina L. Callahan (2021, in press). Skew Surge and Storm
684 Tides of Tropical Storms in the Delaware and Chesapeake Bays for 1980- 2019. *Frontiers in*
685 *Climate: Climate Risk Management*.

686 Callahan, J. A., Horton, B. P., Nikitina, D. L., Sommerfield, C. K., McKenna, T. E., and Swallow, D.
687 (2017). Recommendation of Sea-Level Rise Planning Scenarios for Delaware: Technical Report,
688 prepared for Delaware Department of Natural Resources and Environmental Control (DNREC)
689 Delaware Coastal Programs. 116 pp. DOI:10.13140/RG.2.2.17411.66082

690 [CCPR] Council on Climate Preparedness and Resilience. (2016). Opportunities to Enhance the
691 Nation's Resilience to Climate Change. 46 pp.

692 Chesapeake Bay Program (2020). State of the Chesapeake. https://www.chesapeakebay.net/state
693 [Accessed August 18, 2020].

694 Chippy, M. R., and Jawahar, S. S. (2018). Storm Surge and its Effect-A Review on Disaster
695 Management in Coastal Areas. *Civil Engineering Research Journal*, 4:5, 555649.
696 DOI:10.19080/CERJ.2018.04.555649

697 Codiga, D.L. (2011). Unified Tidal Analysis and Prediction Using the UTide Matlab Functions.
698 Graduate School of Oceanography, University of Rhode Island, GSO Technical Report 2011-01, 60
699 pp.

700 Coles, S. (2001). An Introduction to Statistical Modeling of Extreme Values, 208 pp, Springer,
701 London, DOI:10.1007/978-1-4471-3675-0, 2001

702 Colle, B. A., Booth, J. F., and Chang, E. K. M. (2015). A Review of Historical and Future Changes
703 of Extratropical Cyclones and Associated Impacts along the US East Coast, Current Climate Change
704 Reports, 1(3):125-143. DOI:10.1007/s40641-015-0013-7

705 Dahl, Kristina A., Fitzpatrick, Melanie F., Spanger-Siegfried, Erika (2017). Sea level rise drives
706 increased tidal flooding frequency at tide gauges along the U.S. East and Gulf Coasts: Projections for
707 2030 and 2045. *PLoS One*, 12, 2.

708 Dupigny-Giroux, L.A., E.L. Mecray, M.D. Lemcke-Stampone, G.A. Hodgkins, E.E. Lentz, K.E.
709 Mills, E.D. Lane, R. Miller, D.Y. Hollinger, W.D. Solecki, G.A. Wellenius, P.E. Sheffield, A.B.
710 MacDonald, and C. Caldwell (2018). Northeast. In Impacts, Risks, and Adaptation in the United
711 States: Fourth National Climate Assessment, Volume II [Reidmiller, D.R., C.W. Avery, D.R.
712 Easterling, K.E. Kunkel, K.L.M. Lewis, T.K. Maycock, and B.C. Stewart (eds.)]. U.S. Global
713 Change Research Program, Washington, DC, USA, pp. 669–742. DOI:10.7930/NCA4.2018.CH18

714 Ellis, J. T., and Sherman, D. J. (2015). Perspectives on Coastal and Marine Hazards and Disasters, in
715 Coastal Marine Hazards, Risks, and Disasters [John F. Shroder, Jean T. Ellis, and Douglas J.
716 Sherman, eds]. DOI:10.1016/B978-0-12-396483-0.01001-3

717 Ezer, Tal, Larry P. Atkinson, William B. Corlett, and Jose L. Blanco (2013). Gulf Stream's induced
718 sea level rise and variability along the U.S. mid-Atlantic coast. *Journal of Geophysical Research:*
719 *Oceans*. 118, 2, 685-697, DOI:10.1002/jgrc.20091

720 G'Sell, M.G., Wager, S., Chouldechova, A., Tibshirani, R. (2016). Sequential selection procedures
721 and false discovery rate control. *Journal of the Royal Statistical Society*, Series B (Statistical
722 Methodology), 423 – 444. DOI:10.1111/rssb.12122

723 Guedes Soares, C., Scotto, M.G.: Application of the r largest-order statistics

724 Garner, Andra J., et al. (2017). Impact of climate change on New York City's coastal flood hazard:
725 Increasing flood heights from the preindustrial to 2300 CE. *Proceedings of the National Academy of*
726 *Science USA*, 114:11861–11866.

727 Grinsted, Aslak, John C. Moore, and Svetlana Jevrejeva, 2012. Homogeneous record of Atlantic
728 hurricane surge threat since 1923. *PNAS*, 109, 48, 19601-19605. DOI:10.1073/pnas.1209542109

729 Grinsted, A. and Christensen, J. H. (2021). The transient sensitivity of sea level rise, *Ocean Science*,
730 17, 181–186, DOI:10.5194/os-17-181-2021

731 Hall, J.A., S. Gill, J. Obeysekera, W. Sweet, K. Knuuti, and J. Marburger (2016). Regional Sea Level
732 Scenarios for Coastal Risk Management: Managing the Uncertainty of Future Sea Level Change and
733 Extreme Water Levels for Department of Defense Coastal Sites Worldwide. U.S. Department of
734 Defense, Strategic Environmental Research and Development Program. 224 pp.

735 Hallegatte, S., Green, C., Nicholls, R. J., and Corfee-Morlot, J. (2013). Future flood losses in major
736 coastal cities. *Nature Climate Change*. 3, 802.

737 Hamlington, B.D., Leben, R.R., Kim, K.-Y., Nerem, R.S., Atkinson, L.P., and Thompson, P.R.
738 (2015). The effect of the El Niño-Southern Oscillation on U.S. regional and coastal sea level. *Journal*
739 *of Geophysical Research: Oceans*, 120:3970– 3986, DOI:10.1002/2014JC010602

740 Harris, D. L. (1991). Reproducibility of the harmonic constants. Tidal Hydrodynamics, in B. P.
741 Parker, Ed., John Wiley and Sons, 753–771.

742 Hinkel, J. et al. (2014). Coastal flood damage and adaptation costs under 21st century sea-level rise.
743 *Proceedings of the National Academy of Science USA,* 111, 3292–3297.

744 Hirsch, M.E., Degaetano, A.T., and Colucci, S. J. (2001). An East Coast Winter Storm Climatology.
745 *Journal of Climate*, 14, 882-899. DOI:10.1175/1520-0442(2001)014<0882:AECWSC>2.0.CO;2
746
747 Holgate, S. J., Matthews, A., Woodworth, P. L., Rickards, L. J., Tamisiea, M. E., Bradshaw, E.,
748 Foden, P. R., Gordon, K. M., Jevrejeva, S., and Pugh, J. (2013). New Data Systems and Products at
749 the Permanent Service for Mean Sea Level. *Journal of Coastal Research*, 29, 3, 493 – 504.
750 DOI:10.2112/JCOASTRES-D-12-00175.1

751 Jay, A., D.R. Reidmiller, C.W. Avery, D. Barrie, B.J. DeAngelo, A. Dave, M. Dzaugis, M. Kolian,
752 K.L.M. Lewis, K. Reeves, and D. Winner (2018). Overview. In Impacts, Risks, and Adaptation in the
753 United States: Fourth National Climate Assessment, Volume II [Reidmiller, D.R., C.W. Avery, D.R.
754 Easterling, K.E. Kunkel, K.L.M. Lewis, T.K. Maycock, and B.C. Stewart (eds.)]. U.S. Global
755 Change Research Program, Washington, DC, USA, pp. 33–71. DOI:10.7930/NCA4.2018.CH1

756 Knutson, T., Camargo, S. J., Chan, J. C. L., Emanuel, K., Ho, C-H., Kossin, James, Mohapatra, M.,
757 Satoh, M., Sugi, M., Walsh, K., and Wu, L. (2019). Tropical Cyclones and Climate Change

758 Assessment: Part I: Detection and Attribution. *Bulletin of the American Meteorological Society*,
759 1987-2007.

760 Knutson, T., Camargo, S. J., Chan, J. C. L., Emanuel, K., Ho, C-H., Kossin, J., Mohapatra, M., Satoh
761 M., Sugi, M., Walsh, K., and Wu, L. (2020). Tropical Cyclones and Climate Change Assessment:
762 Part II: Projected Response to Anthropogenic Warming. *Bulletin of the American Meteorological*
763 *Society*, E303-E322. DOI:10.1175/BAMS-D-18-0194.1

764 Kopp, Robert E., Gilmore, Elisabeth A., Little, Christopher M., Lorenzo-Trueba, Jorge, Ramenzoni,
765 Victoria C., and Sweet, William V. (2019). Usable Science for Managing the Risks of Sea-Level
766 Rise. *Earth's Future*, 7, 1235 – 1269, DOI:10.1029/2018EF001145

767 Kopp, R. E., Hayhoe, K., Easterling, D. R., Hall, T., Horton, R., Kunkel, K.E., and LeGrande, A.N.
768 (2017). Potential surprises – compound extremes and tipping elements. In: Climate Science Special
769 Report: Fourth National Climate Assessment, Volume I [Wuebbles, D.J., D.W. Fahey, K.A. Hibbard,
770 D.J. Dokken, B.C. Stewart, and T.K. Maycock (eds.)]. U.S. Global Change Research Program,
771 Washington, DC, USA, pp. 411-429, DOI:10.7930/J0GB227J

772 Kopp, R. E. (2013). Does the mid-Atlantic United States sea level acceleration hot spot reflect ocean
773 dynamic variability? *Geophysical Research Letters*, 40:3981–3985. DOI:10.1002/grl.50781

774 Kossin, J. P., Hall, T., Knutson, T., Kunkel, K. E., Trapp, R. J., Waliser, D. E., and Wehner, M. F.
775 (2017). Extreme storms. In: Climate Science Special Report: Fourth National Climate Assessment,
776 Volume I [Wuebbles, D. J., Fahey, D. W., Hibbard, K. A., Dokken, D. J., Stewart, B. C., and
777 Maycock, T. K. (eds.)]. U.S. Global Change Research Program, Washington, DC, USA, pp. 257-276.
778 DOI:10.7930/J07S7KXX

779 Kossin, J. P. (2018). A global slowdown of tropical-cyclone translation speed. *Nature*, 558:104–107.
780 DOI:10.1038/s41586-018-0158-3

781 Lee., S. B., Li, M., and Zhang, F. (2017). Impact of sea level rise on tidal range in Chesapeake and
782 Delaware Bays. *Journal of Geophysical Research: Oceans*, 122, 3917-3938.
783 DOI:10.1002/2016JC012597

784 Lin, Ning, Kopp, Robert E., Horton, Benjamin P., and Donnelly, Jeffery P. (2016). Hurricane
785 Sandy's flood frequency increasing from 1800 to 2100. *Proceedings of the National Academy of*
786 *Science*, USA, 14(33): 12071–12075, DOI:10.1073/pnas.1604386113

787 Little, Christopher M., Hu, Aixue, Hughes, Chris W., McCarthy, Gerard D., Piecuch, Christopher G.,
788 Ponte, Rui M., Thomas, Matthew D. (2019). The Relationship Between U.S. East Coast Sea Level
789 and the Atlantic Meridional Overturning Circulation: A Review, *Journal of Geophysical Research:*
790 *Oceans*, 124:9, DOI:10.1029/2019JC015152

791 Mawdsley, R. J., and Haigh, I. D. (2016). Spatial and Temporal Variability and Long-Term Trends in
792 Skew Surges Globally. *Frontiers in Marine Science*, 3, 1-29. DOI:10.3389/fmars.2016.00029

793 Moftakhari, H. R., AghaKouchak, A., Sanders, B. F., and Matthew, R. A. (2017). Cumulative hazard:
794 the case of nuisance flooding. *Earth's Future,* 5, 214–223. DOI:10.1002/2016ef000494

795 Moftakhari, H. R., AghaKouchak, A., Sanders, B. F., Feldman, D. L., Sweet, W., Matthew, R. A.,
796 and Luke, A. (2015). Increased nuisance flooding along the coasts of the United States due to sea
797 level rise: Past and future. *Geophysical Research Letters*, 42, 9846–9852.
798 DOI:10.1002/2015GL066072

799 Morton, R. A., Guy, K. K., Hill, H. W., and Pascoe, T. (2003). Regional morphological responses to
800 the March 1962 Ash Wednesday storm. *Proceedings Coastal Sediments '03*, 11pp.

801 Muis S., Irazoqui, Apecechea M., Dullaart, J., de Lima, Rego J., Madsen, K.S., Su, J., Yan, K., and
802 Verlaan, M. (2020). A High-Resolution Global Dataset of Extreme Sea Levels, Tides, and Storm
803 Surges, Including Future Projections. Frontiers in Marine Science, 7:263.
804 DOI:10.3389/fmars.2020.00263

805 Murakami, H., Delworth, T. L., Cooke, W. F., Zhao, M., Xiang, B., and Hsu, P. C. (2020). Detected
806 climatic change in global distribution of tropical cyclones. *PNAS*, 117:20, 10706-10714.
807 DOI:10.1073/pnas.1922500117

808 NOAA CO-OPS (2020a). NOAA National Ocean Service Center for Operational Oceanographic
809 Products and Services (CO-OPS). Sea Level Trends. https://tidesandcurrents.noaa.gov/sltrends/
810 [Accessed August 18, 2020].

811 NOAA CO-OPS (2020b). NOAA National Ocean Service Center for Operational Oceanographic
812 Products and Services (CP-OPS). API for Data Retrieval.
813 https://api.tidesandcurrents.noaa.gov/api/prod/ [Accessed April 9, 2020].

814 NOAA CO-OPS (2020c). NOAA National Ocean Service Center for Operational Oceanographic
815 Products and Services (CO-OPS). NOAA Tide Predictions.
816 https://tidesandcurrents.noaa.gov/tide_predictions.html [Accessed April 9, 2020].

817 NOAA CO-OPS (2007). Tidal Analysis and Prediction, NOAA Special Publication National Ocean
818 Service (NOS) Center for Operational Oceanographic Products and Services (CO-OPS) 3, 388 pp.

819 NOAA NCEI (2020). U.S. Billion-Dollar Weather and Climate Disasters. NOAA National Centers
820 for Environmental Information (NCEI). DOI:10.25921/stkw-7w73

821 NOAA NWLON (2020). NOAA National Ocean Service National Water Level Observation Network
822 (NWLON). https://www.tidesandcurrents.noaa.gov/nwlon.html [Accessed August 18, 2020].

823 NOAA PORTS (2020). National Ocean Service Physical Oceanographic Real-Time System
824 (PORTS). https://tidesandcurrents.noaa.gov/ports.html [Accessed August 18, 2020].

825 Oppenheimer, M., Glavovic, B. C., Hinkel, J., van de Wal, R., Magnan, A. K., Abd-Elgawad, A., et
826 al. (2019). "Sea level rise and implications for low-lying islands, coasts and communities," in IPCC
827 Special Report on the Ocean and Cryosphere in a Changing Climate, eds H.-O. Pörtner, D. C.
828 Roberts, V. Masson-Delmotte, P. Zhai, M. Tignor, E. Poloczanska, et al.

829 [PDE] Partnership for the Delaware Estuary (2017). Technical Report for the Delaware Estuary and
830 Basin 2017. L. Haaf,, S. Demberger, D. Kreeger, and E. Baumbach (eds). PDE Report No. 17-07.
831 379 pages.

832 Piecuch, C. G., P. Huybers, C. C. Hay, A. C. Kemp, C. M. Little, J. X. Mitrovica, R. M. Ponte, and
833 M. P. Tingley (2018). Origin of spatial variation in US East Coast sea-level trends during 1900–
834 2017. *Nature*, 564, 400-404. DOI:10.1038/s41586-018-0787-6.

835 Pugh, D., and Woodworth, P. (2014). Sea-Level Science: Understanding Tides, Surges, Tsunamis
836 and Mean Sea-Level Changes. Cambridge: Cambridge University Press.
837 DOI:10.1017/CBO9781139235778

838 Rahmstorf, S. (2017). Rising hazard of storm-surge flooding. *PNAS Commentary*, 114:45, 11806-
839 11808. DOI:10.1073/pnas.1715895114

840 Rappaport, E. (2014). Fatalities in the United States from Atlantic Tropical Cyclones New Data and
841 Interpretation. *Bulletin of the American Meteorological Society Insights and Innovations*. 341 – 346.

842 Rashid, Md. Mamunur, Wahl, Thomas, Chambers, Don P., Calafat, Francisco M., and Sweet,
843 William V. (2019). An extreme sea level indicator for the contiguous United States coastline.
844 *Scientific Data*, 6, 326, DOI:10.1038/s41597-019-0333-x

845 Ribatet, Mathieu, and Dutang, Christopher (2019). POT: Generalized Pareto Distribution and Peaks
846 Over Threshold. R package version 1.1-7.

847 Ross, A. C., Najjar, R. G., Li, M., Lee, S. B., Zhang, F., and Liu, W. (2017). Fingerprints of sea level
848 rise on changing tides in the Chesapeake and Delaware Bays. *Journal of Geophysical Research:*
849 *Oceans*, 122, 8102–8125. https://doi.org/10.1002/2017JC012887

850 Sallenger, A. H., Doran, K. S., and Howd, P. A. (2012). Hotspot of accelerated sea-level rise on the
851 Atlantic coast of North America. *Nature Climate Change*, 2, 884–888, DOI:10.1038/nclimate1597

852 Sanchez, J. R., Kauffman, G., Reavy, K., Homsey, A. (2012). "Chapter 1.7 - Natural Capital Value"
853 in the Technical Report for the Delaware Estuary and Basin. Partnership for the Delaware Estuary.
854 PDE Report No.17-07 pp. 70-75.

855 Scarrott, Carl, and MacDonald, Anna, 2012. A Review of Extreme Value Threshold Estimation and
856 Uncertainty Quantification. *Statistical Journal*, 10, 1, 33-60.

857 Smith, A., 2021. 2020 U.S. billion-dollar weather and climate disasters in historical context,
858 Technical Report. DOI:10.13140/RG.2.2.25871.00166/1

859 Stephens, S. A., Bell, R. G., and Haigh, I. D. (2020). Spatial and temporal analysis of extreme storm-
860 tide and skew-surge events around the coastline of New Zealand. *Natural Hazards and Earth System*
861 *Sciences*, 20, 3, 783-796.

862 Sweet, W., Dusek, G., Carbin, G., Marra, J., Marcy, D., and Simon, S. (2020). 2019 State of U.S.
863 High Tide Flooding with a 2020 Outlook. NOAA Technical Report NOS CO-OPS 092, 24 pp.

864 Sweet, W. V., Dusek, G., Obeysekera, J., and Marra, J. J. (2018). Patterns and Projections of High
865 Tide Flooding Along the U.S. Coastline Using a Common Impact Threshold. NOAA Technical
866 Report NOS CO-OPS 086, 56 pp.

867 Sweet, W. V., Horton, R. M., Kopp, R. E., LeGrande, A. N., and Romanou, A. (2017a). Sea level
868 rise. In: Climate Science Special Report: Fourth National Climate Assessment, Volume I [Wuebbles,
869 D.J., D.W. Fahey, K.A. Hibbard, D.J. Dokken, B.C. Stewart, and T.K. Maycock (eds.)]. U.S. Global
870 Change Research Program, Washington, DC, USA, pp. 333-363. DOI:10.7930/J0VM49F2.

871 Sweet, W. V., Kopp, R. E., Weaver, C. P., Obeysekera, J., Horton, R. M., Thieler, E. R., and Zervas,
872 C. (2017b). Global and Regional Sea Level Rise Scenarios for the United States. NOAA Technical
873 Report NOS CO-OPS 083, 75 pp.

874 Sweet, W. V., Park, J., Marra, J. J., Zervas, C. E., and Gill, S. (2014). Sea Level Rise and Nuisance
875 Flood Frequency Changes around the United States. NOAA Technical Report NOS CO-OPS 073, 66
876 pp.

877 Taherkhani, M., Vitousek, S., Barnard, P., Frazer, N., Anderson, T., & Fletcher, C. (2020). Sea-level
878 rise exponentially increases coastal flood frequency. Scientific Reports, 10.

879 Tawn, Jonathon A. (1988). An extreme-value theory modle for dependent observations. *Journal of*
880 *Hydrology*, 101, 227-250.

881 Tebaldi, C., Strauss, B. H., and Zervas, C. E. (2012). Modeling sea level rise impacts on storm surges
882 along US coasts. *Environmental Research Letters*, 7, 014032.

883 Thompson, P. R., G. T. Mitchum, C. Vonesch, and J. Li, 2013. Variability of winter storminess in the
884 eastern United States during the twentieth century from tide gauges. *Journal of Climatology*, 26,
885 9713–9726, DOI:10.1175/JCLI-D-12-00561.1

886 [USACE] US Army Corps of Engineers. (2014). North Atlantic Coast Comprehensive Study
887 (NACCS), State Chapter D-7: State of Delaware, 142 pp.

888 Walton, Todd L. Jr. (2000). Distributions for storm surge extremes. *Ocean Engineering*, 27, 1279 –
889 1293.

890 Wang, Shuai and Toumi, Ralf (2021). Recent migration of tropical cyclones toward coasts. *Science*,
891 371, 6528, 514-517. DOI:10.1126/science.abb9038

892 Wahl, T. and Chambers, D. P. (2015). Evidence for multidecadal variability in US extreme sea level
893 records. *Journal Geophysical Research: Oceans*, 120, 1527–1544

894 Wahl, Thomas (2017). Sea-level rise and storm surges, relationship status: complicated!
895 *Environmental Research Letters*, 12, DOI:10.1088/1748-9326/aa8eba

896 Wahl, T., Haigh, I.D., Nicholls, R.J., Arns, A., Dangendorf, S., Hinkel, J., and Slangen, A.B.A.
897 (2017). Understanding extreme sea levels for broad-scale coastal impact and adaptation analysis.
898 Nature Communications, 8, 16075

899 Weinkle, J., Landsea, C., Collins, D., Musulin, R., Crompton, R. P., Klotzbach, P. K., and Pielke R.
900 Jr (2018). Normalized hurricane damage in the continental United States 1900–2017. Nature
901 Sustainability. DOI:10.1038/s41893-018-0165-2

902 Weissman, Ishay (1978). Estimation of parameters and larger quantiles based on the k-largest
903 observations. *Journal of the American Statistical Association*, 73, 364, 812-815.

904 Williams, J., Horsburgh, K. J., Williams, J. A., and Proctor, R. N. F. (2016). Tide and skew surge
905 independence: New insights for flood risk. *Geophysical Research Letters*, 43, 6410–6417.
906 DOI:10.1002/2016GL069522

907 Wong, Tony E., Torline, Travis, and Zhang, Mingxuan (2020). Evidence for increasing frequency of
908 extreme coastal sea levels. arXiv [Preprint]. Available at https://arxiv.org/abs/2006.06804 (Accessed
909 January 29, 2021).

910 Wong, K–C., and Münchow, A. (1995). Buoyancy forced interaction between estuary and inner
911 shelf: observation, *Continental Shelf Research*, 15,1, 59-88.

912 Yang, H., Lohmann, G., Lu, J., Gowan, E.J., Shi, X., Liu, J., Wang, Q. (2020). Tropical expansion
913 driven by poleward advancing mid-latitude meridional temperature gradients, *JGR Atmospheres*.
914 DOI:10.1029/2020JD033158

915 Zhong, L., and Li, M. (2006). Tidal Energy Fluxes and Dissipation in the Chesapeake Bay.
916 *Continental Shelf Research*, 26, 6, 752-770.

917

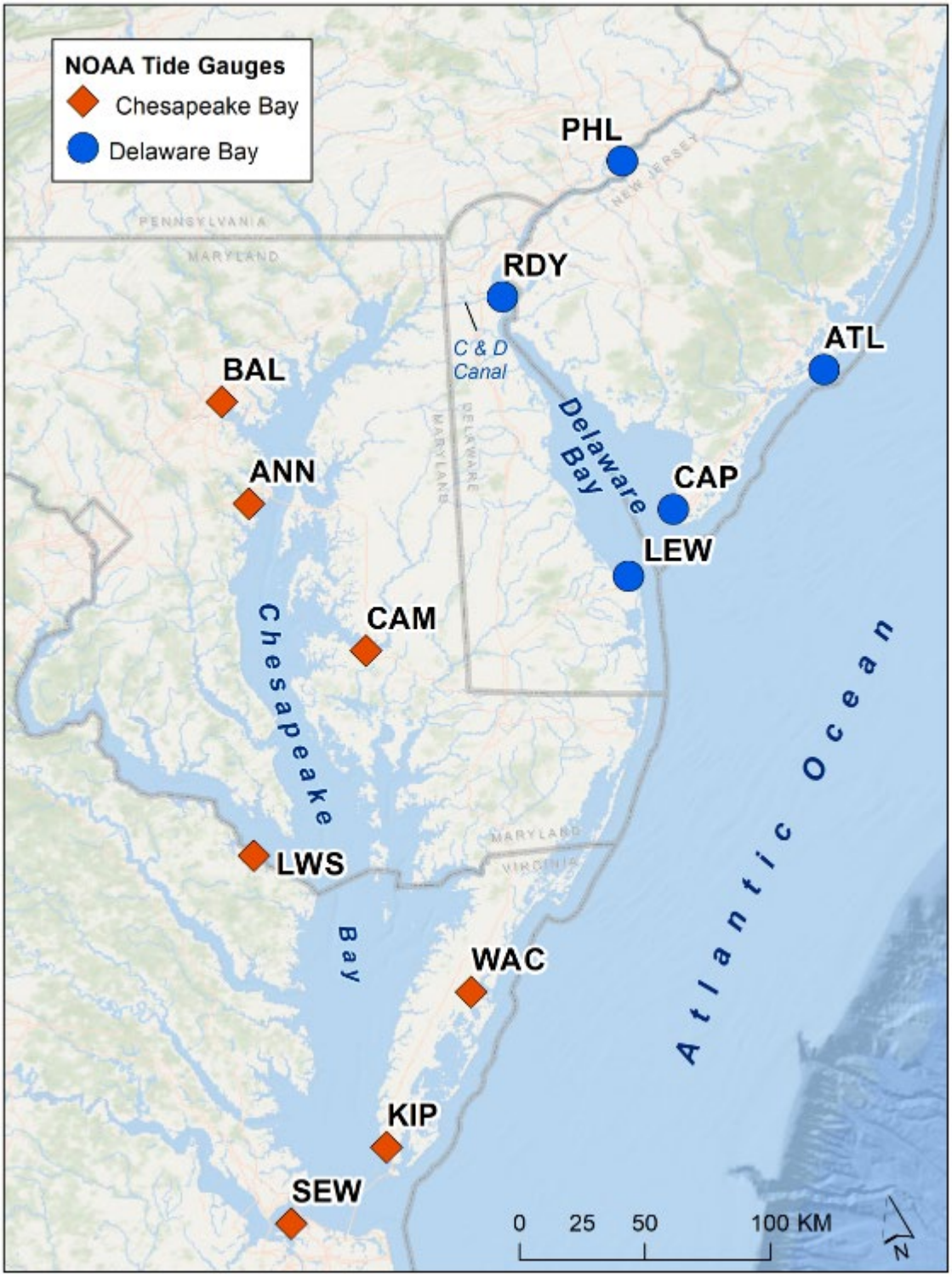

Figure 1. Map of the Delaware and Chesapeake Bays with the 12 NOAA tide gauges used in the current study: Philadelphia (PHL), Reedy Point (RDY), Cape May (CAP), Atlantic City (ATL), Baltimore (BAL), Annapolis (ANN), Cambridge (CAM), Lewisetta (LWS), Kiptopeke (KIP), Sewells Point (SEW), Wachapreague (WAC).

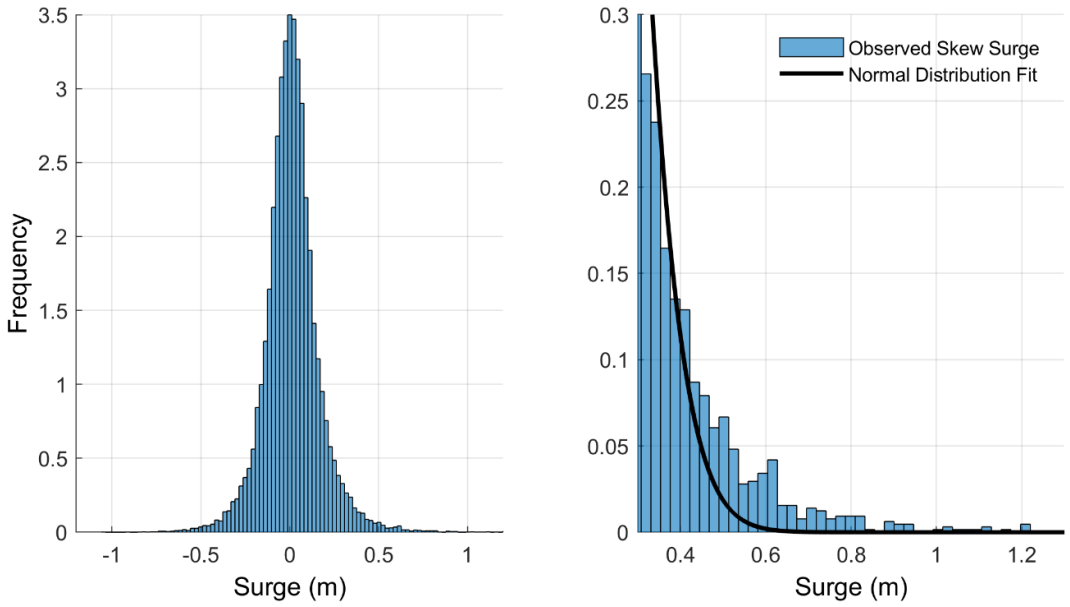

Figure 2. Example demonstrating the "fat tail" nature of skew surge distribution for the NOAA Lewes tide gauge. Histogram includes all detrended skew surges over 1980 – 2019 (left panel, N = 28091). Upper tail of the same data with Normal distribution model fitted to the full parent distribution (right panel). Note the upper tail of the theoretical parent distribution under-represents empirical skew surge.

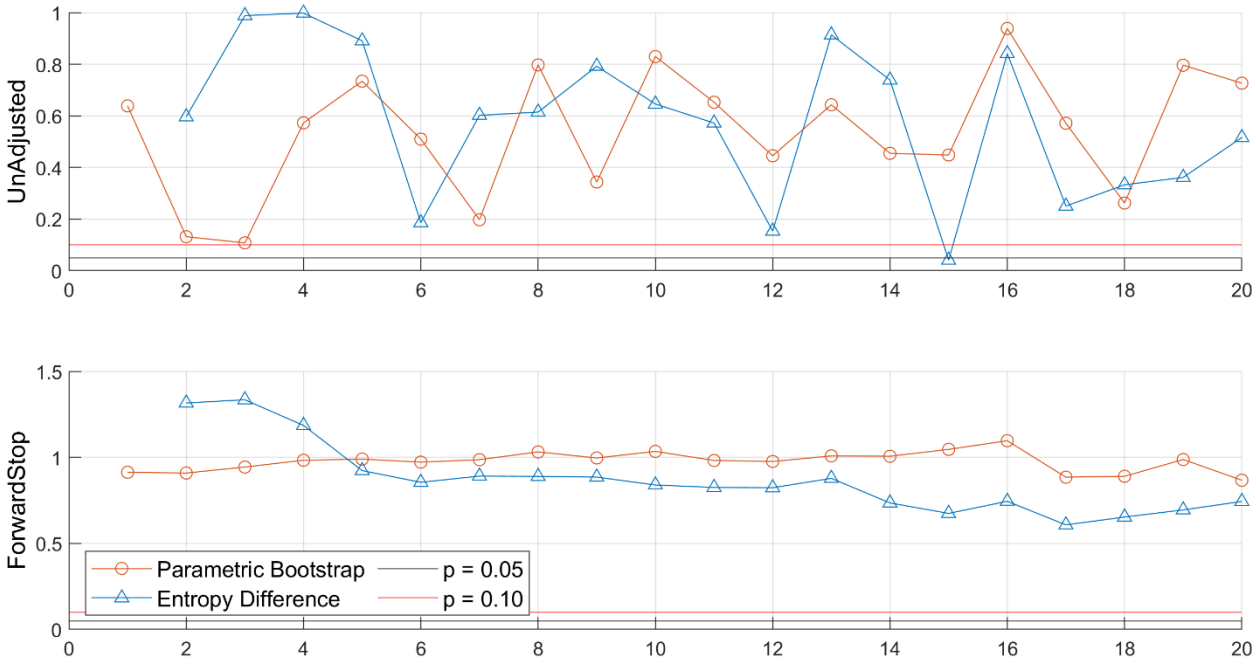

Figure 3. Example demonstrating GEVr Unadjusted p-values (top panel) and ForwardStop (bottom panel) results based on Parametric Bootstrap and Entropy Difference tests for r = 1 – 20, as defined in Bader et al. (2017). Following the guidelines outlined in the current study, optimum r = 14.

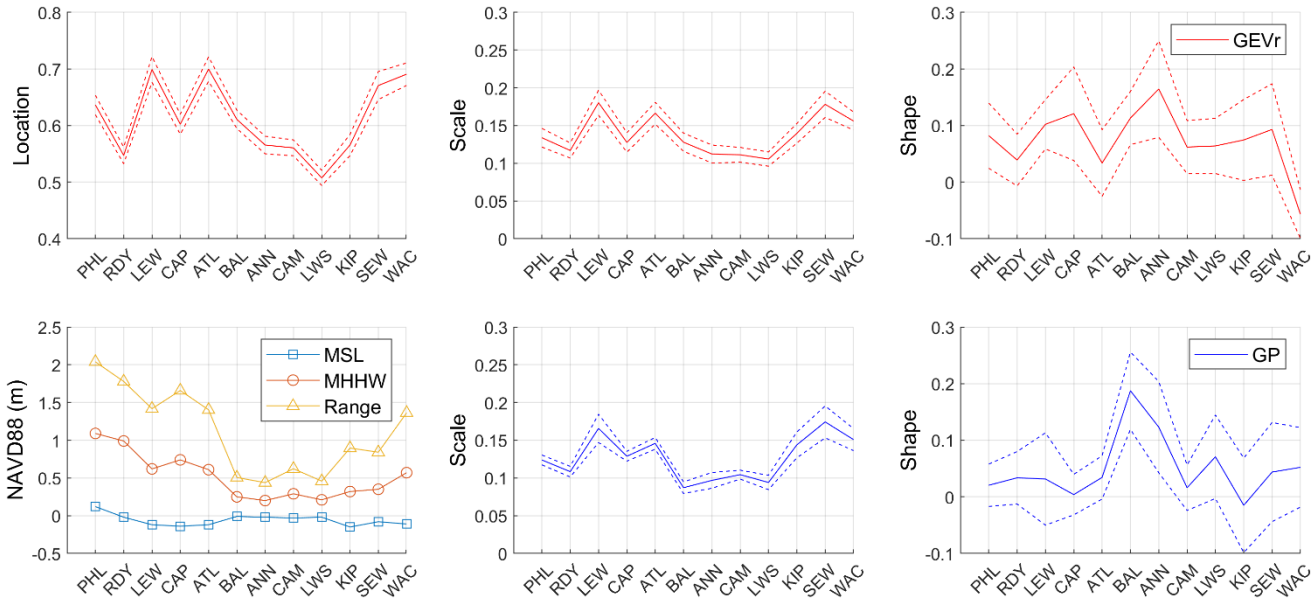

935

936 **Figure 4.** Model fit parameters of extreme skew surges to the GEVr (red, top row) and GP (blue,
937 bottom row) distributions. Location is a model parameter only for GEVr distribution. Dotted lines
938 represent the 90% confidence interval. Mean Sea Level (MSL), Mean Higher-High Water (MHHW),
939 and Great Diurnal Range (GT) tidal datums defined by NOAA for the current National Tidal Datum
940 Epoch (NTDE) 1983-2001 and referenced to NAVD88 meters.

941

942

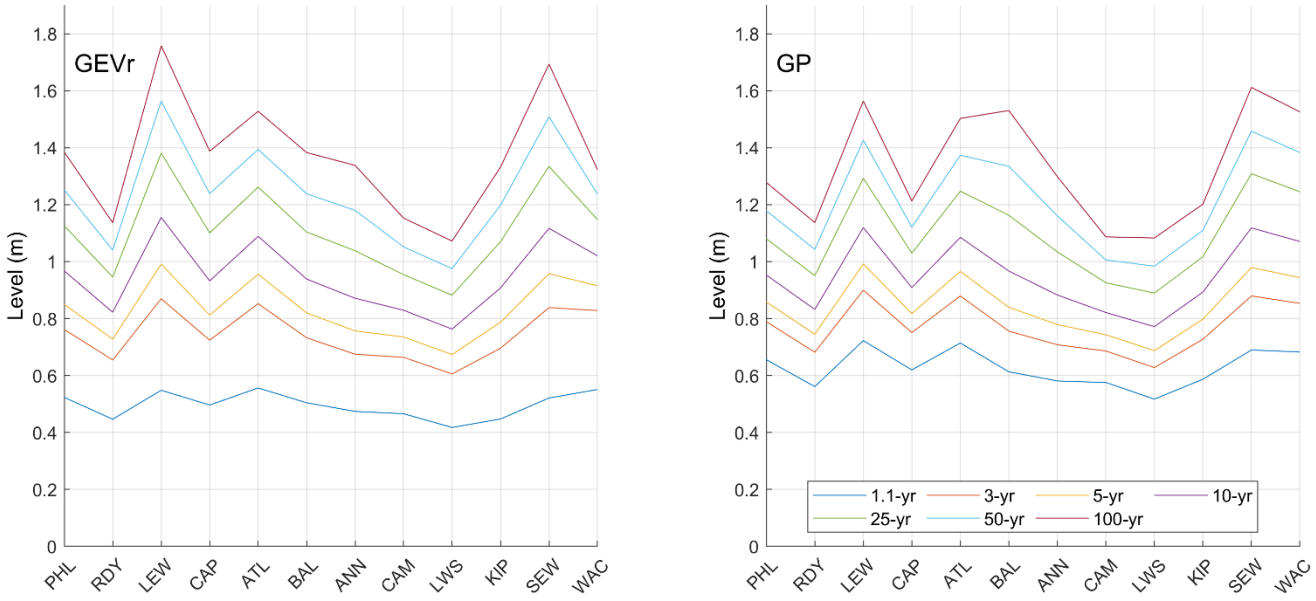

943

944 **Figure 5.** Estimated skew surge for return periods of 1.1, 3, 5, 10, 25, 50, and 100 years using the
945 BM/GEVr (left panel) and POT/GP (right panel) approaches for tide gauges in the Mid-Atlantic
946 region, 1980 – 2019. All data referenced to NAVD88 meters.

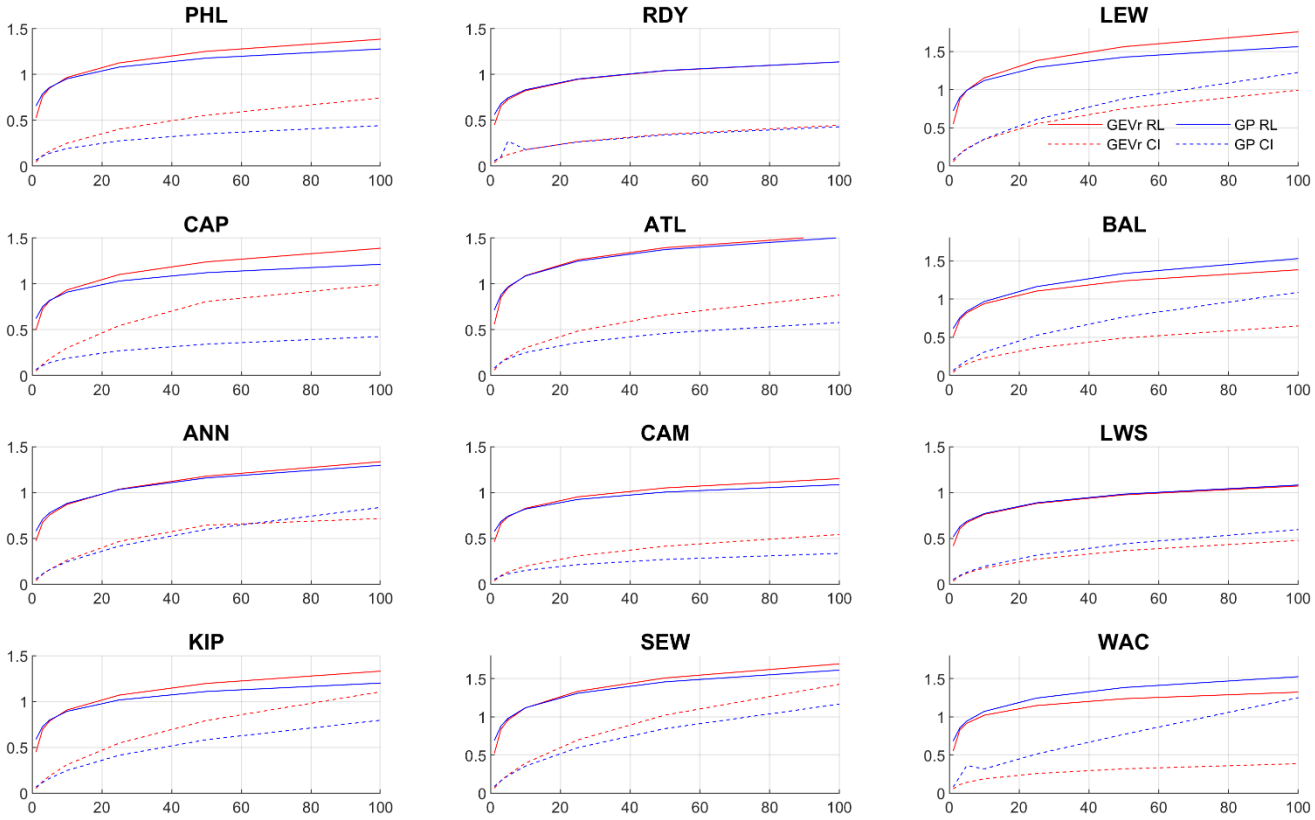

Figure 6. Differences in return levels (solid line) and 90% confidence intervals (dotted line) between the BM/GEVr (red line) and POT/GP (blue line) approaches. All data referenced to NAVD88 meters.

Supplementary Material

1. Supplementary Figures

The following 24 figures represent diagnostic plots for the extreme value distribution model fits of skew surge for each tide gauge. The first set of 12 show results of the BM/GEVr approach using the optimzied value of r, while the second set show results of the POT/GP approach using the optimized threshold. Details on the model fit optimization can be found in the main manuscript sections 2.3 and 2.4. Each figure is composed of four diagnotic plots, in the following layout:

Top left – Probability-Probability plot. Each data point's empirical probability is plotted on the x-axis while it's corresponding probability based on the hypothesized model is plotted on the y-axis. Generally, the closer the points are to the 1-to-1 line, the better the fit.

Top right – Quantile-Quantile plot. Each data point's empirical value is plotted on the x-axis while it's hypothesized value based on it's empirical quantile, is plotted on the y-axis. Similar to the probabiility-probability plot, points along the 1-to-1 line represent a better model fit.

Bottom left – Histogram and Probability Density Function (PDF). The histogram shows the frequency distribution of the data points. When fitting to the GP, the values are exceedances over the selected threshold. The PDF curve represents the extreme value distribution PDF with estimated model parameters (location, scale, and shape for GEVr; scale and shape for GP.) Data point empirical values are plotted based on the magnitude along the x-axis to provide a more exact location of where the points fall within each bin.

Bottom right – Return Level plot. Skew surge return levels are plotted on the y-axis and return periods plotted on the x-axis. The x-axis is plotted on a logrithmic scale from aprroximately 0.1 to 1000 return year time periods. For a return period of 100 years, the corresponding return level has a 1% probability of occurring in any single year. The 90% confidence interval is also plotted, widening for increasing return periods. Since only 40 years of data were compiled to produce the model fits and corresponding return level estimates, the furthest (maximum) empirical data point along the x-axis should lie near the 40-year return period. The more narrow the confidence interval, the more robust the central estimate. As well, the more data points that fall within the confidence intervals, especially if narrow, the more closely larger data points match with the longer return period estimates.

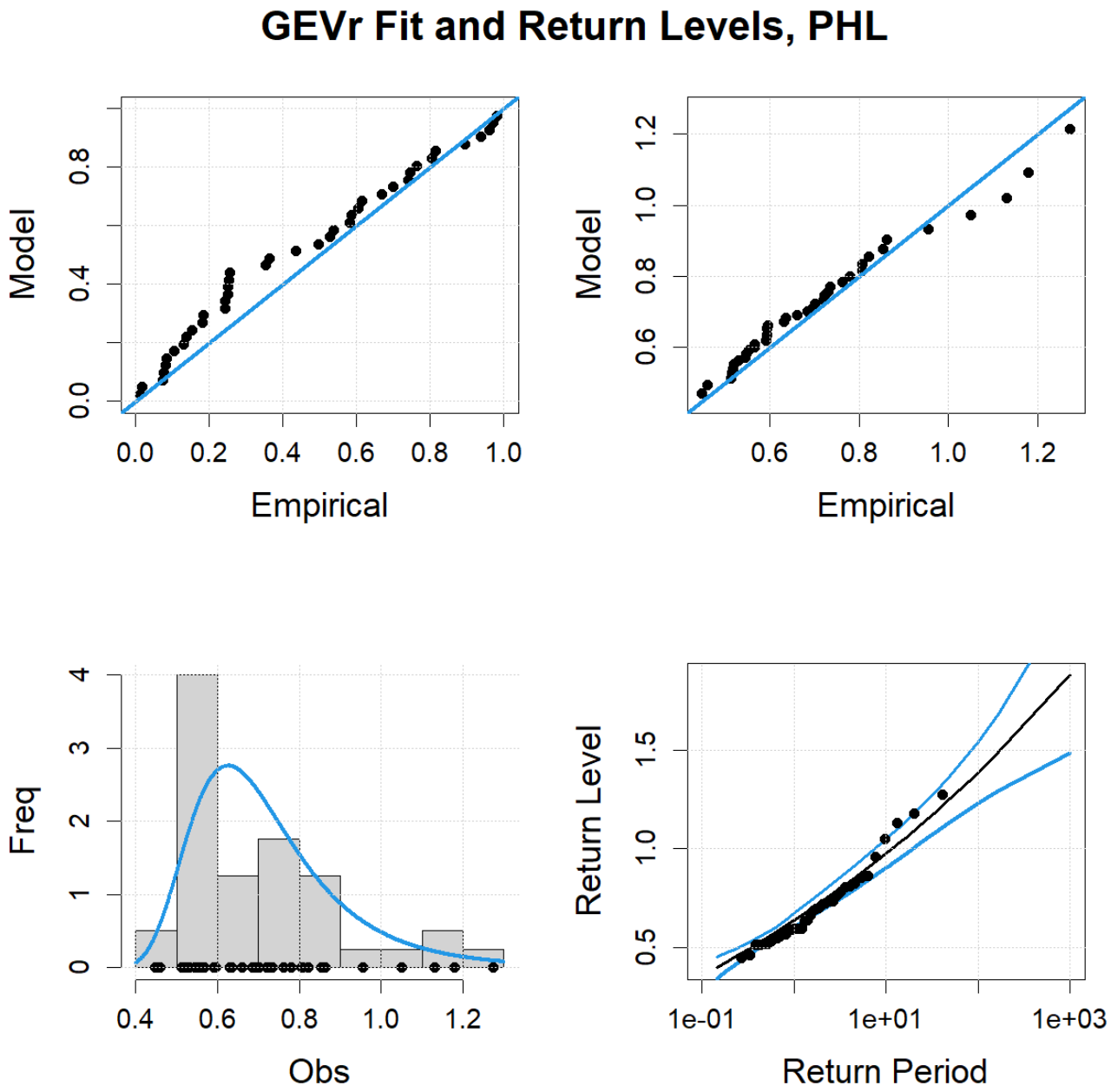

982

983 **Supplementary Figure 1.** Diagnostic plots for extreme skew surge fit to GEVr model at
984 Philadelphia NOAA tide gauge (8545240) in the Delaware River/Bay. (see introduction to this
985 supplementary doc for explanation of plots.)

986

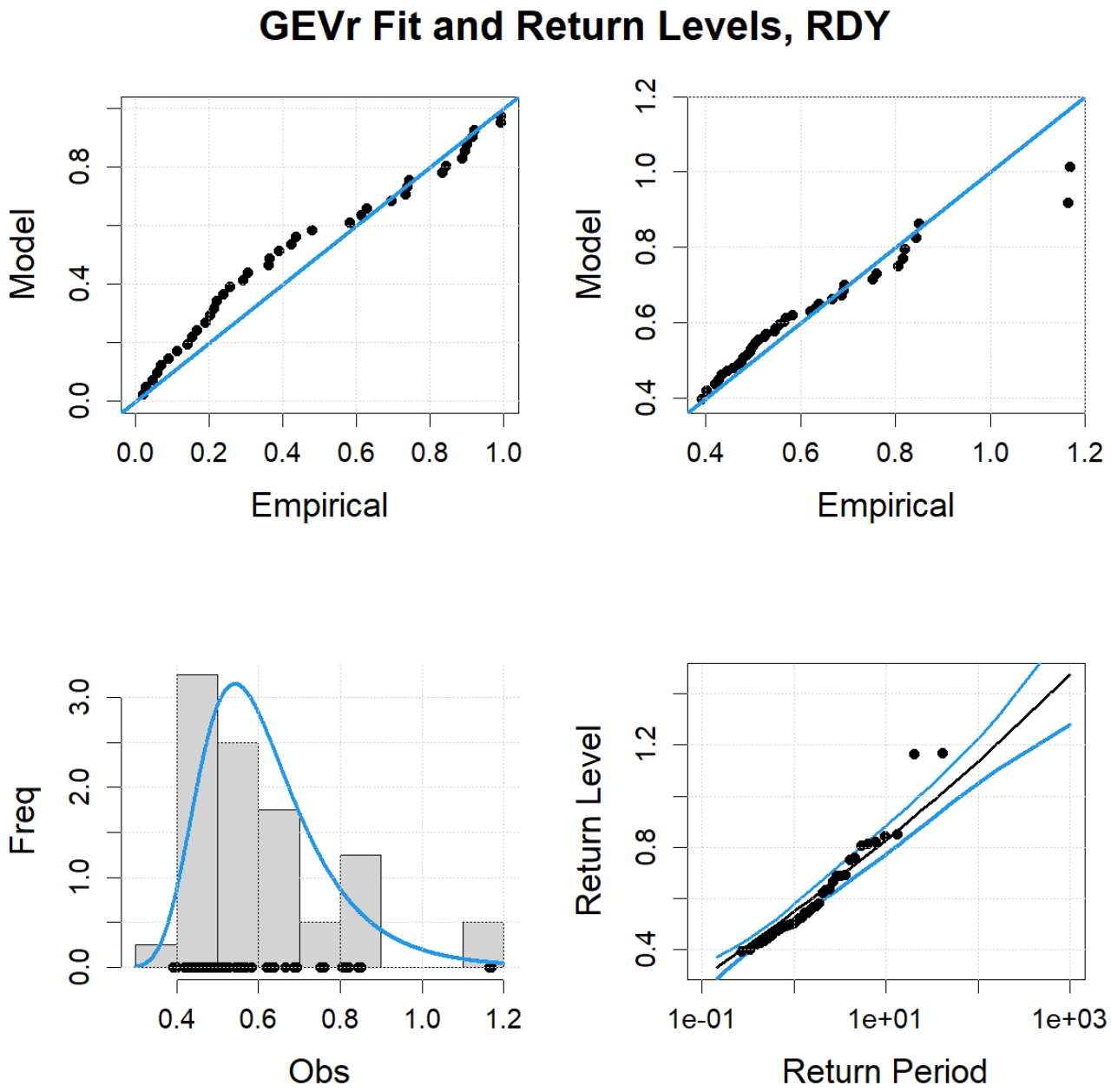

Supplementary Figure 2. Diagnostic plots for extreme skew surge fit to GEVr model at Reedy Point NOAA tide gauge (8551910) in the Delaware Bay. (see introduction to this supplementary doc for explanation of plots.)

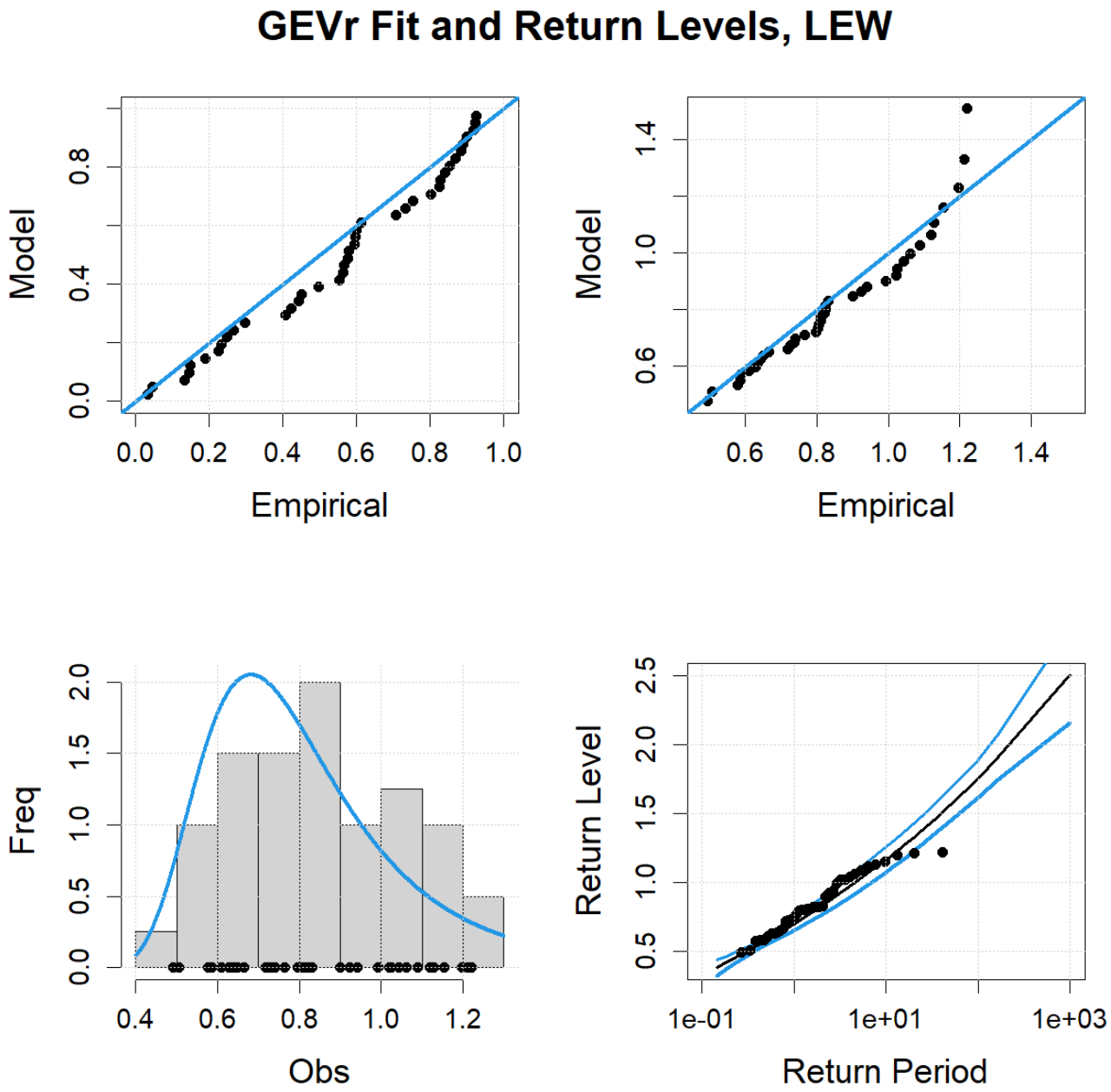

993

994 **Supplementary Figure 3.** Diagnostic plots for extreme skew surge fit to GEVr model at Lewes
995 NOAA tide gauge (8557380) in the Delaware Bay. (see introduction to this supplementary doc for
996 explanation of plots.)

997

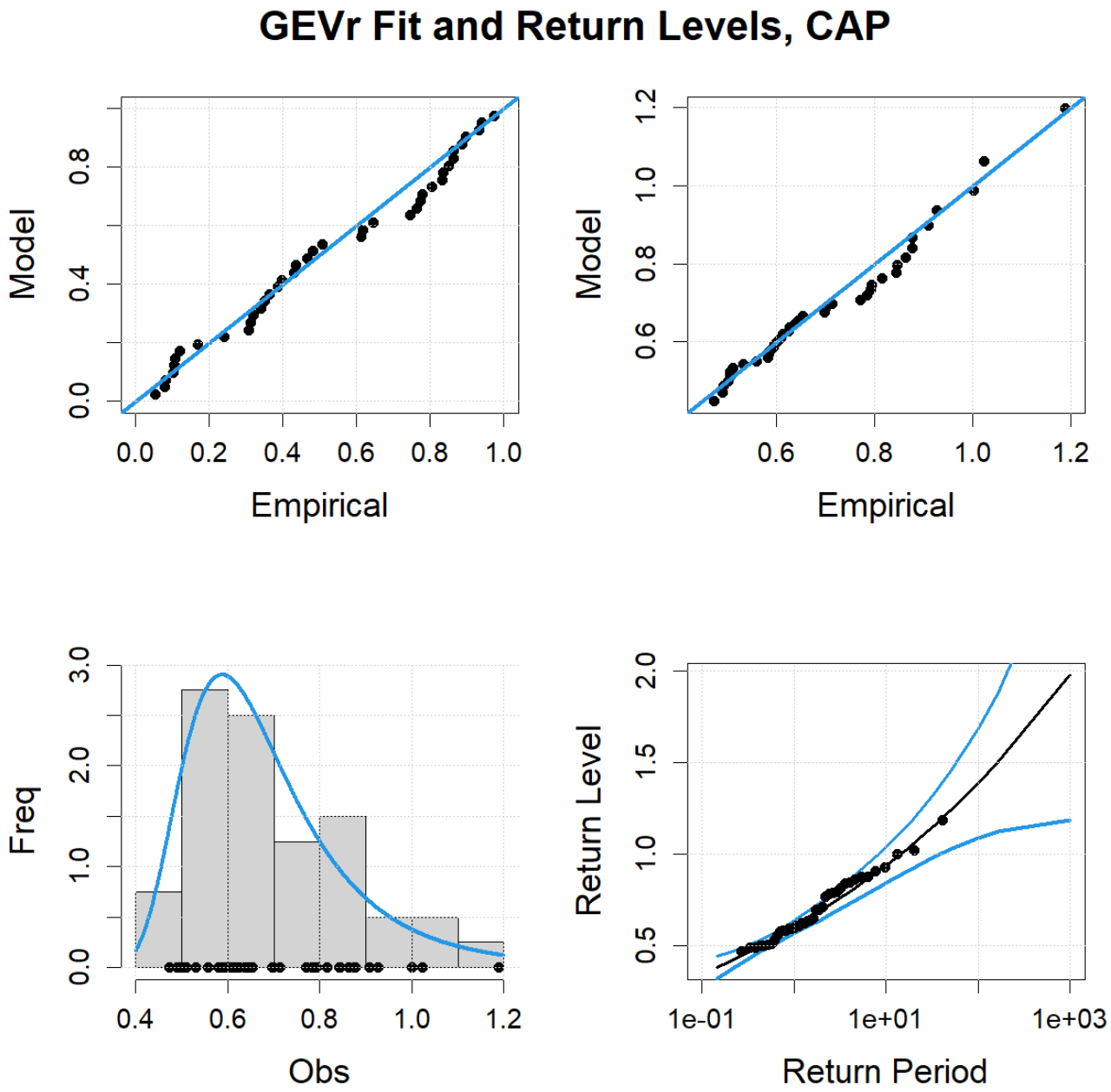

Supplementary Figure 4. Diagnostic plots for extreme skew surge fit to GEVr model at Cape May NOAA tide gauge (8536110) in the Delaware Bay. (see introduction to this supplementary doc for explanation of plots.)

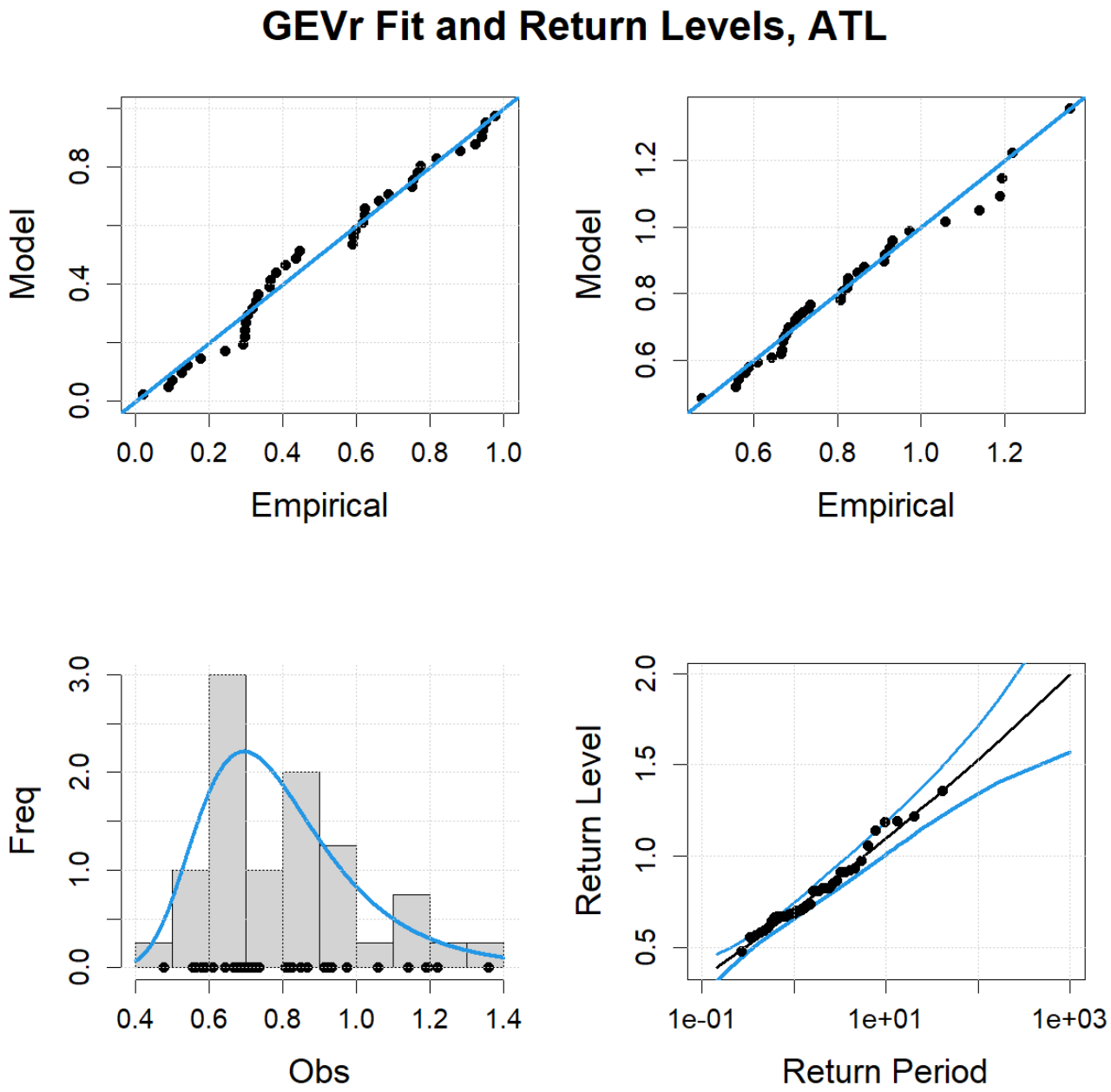

1004

1005 **Supplementary Figure 5.** Diagnostic plots for extreme skew surge fit to GEVr model at Atlantic
1006 City NOAA tide gauge (8534720) near the Delaware Bay. (see introduction to this supplementary
1007 doc for explanation of plots.)

1008

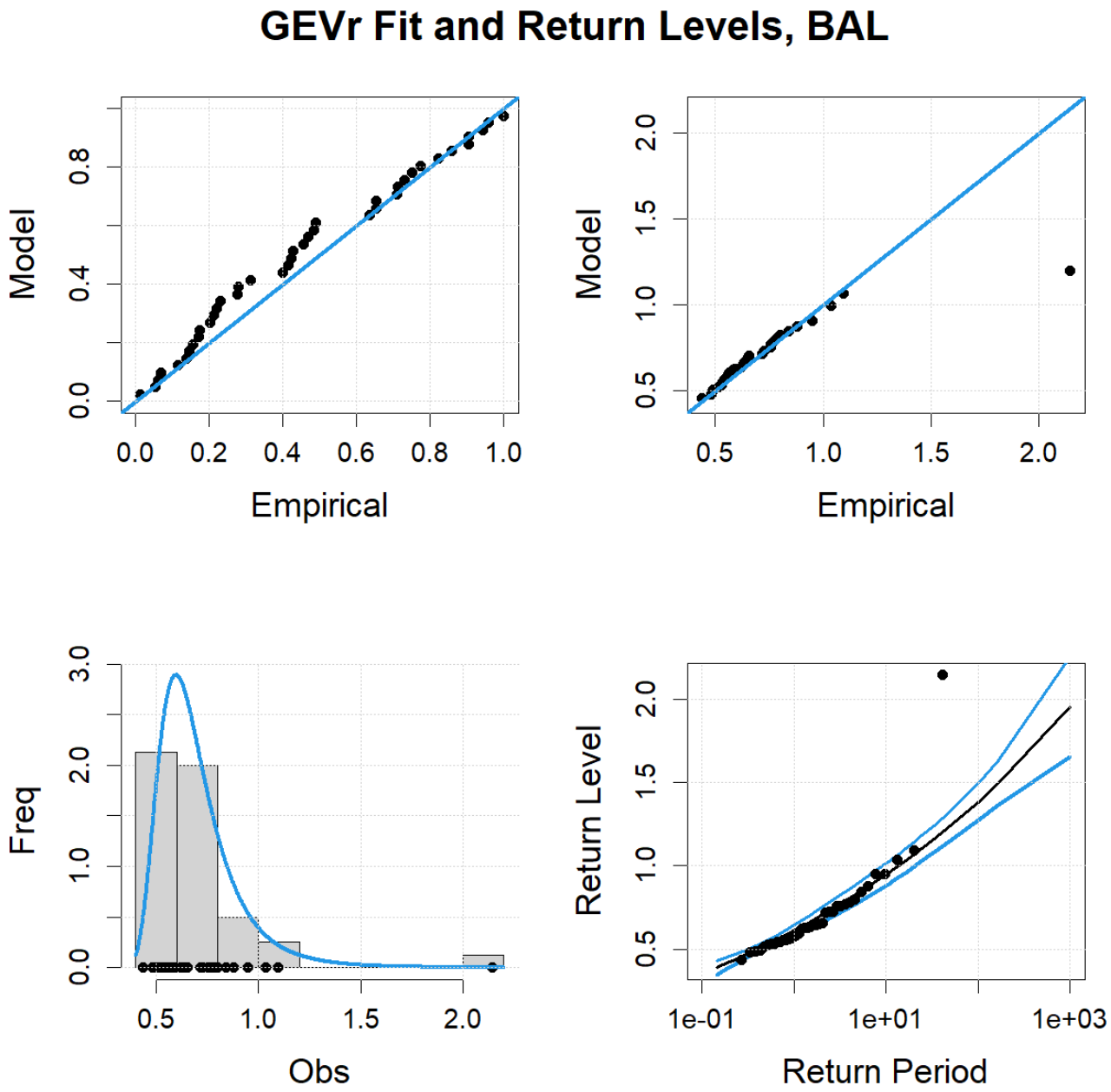

Supplementary Figure 6. Diagnostic plots for extreme skew surge fit to GEVr model at Baltimore NOAA tide gauge (8574680) in the Chesapeake Bay. (see introduction to this supplementary doc for explanation of plots.)

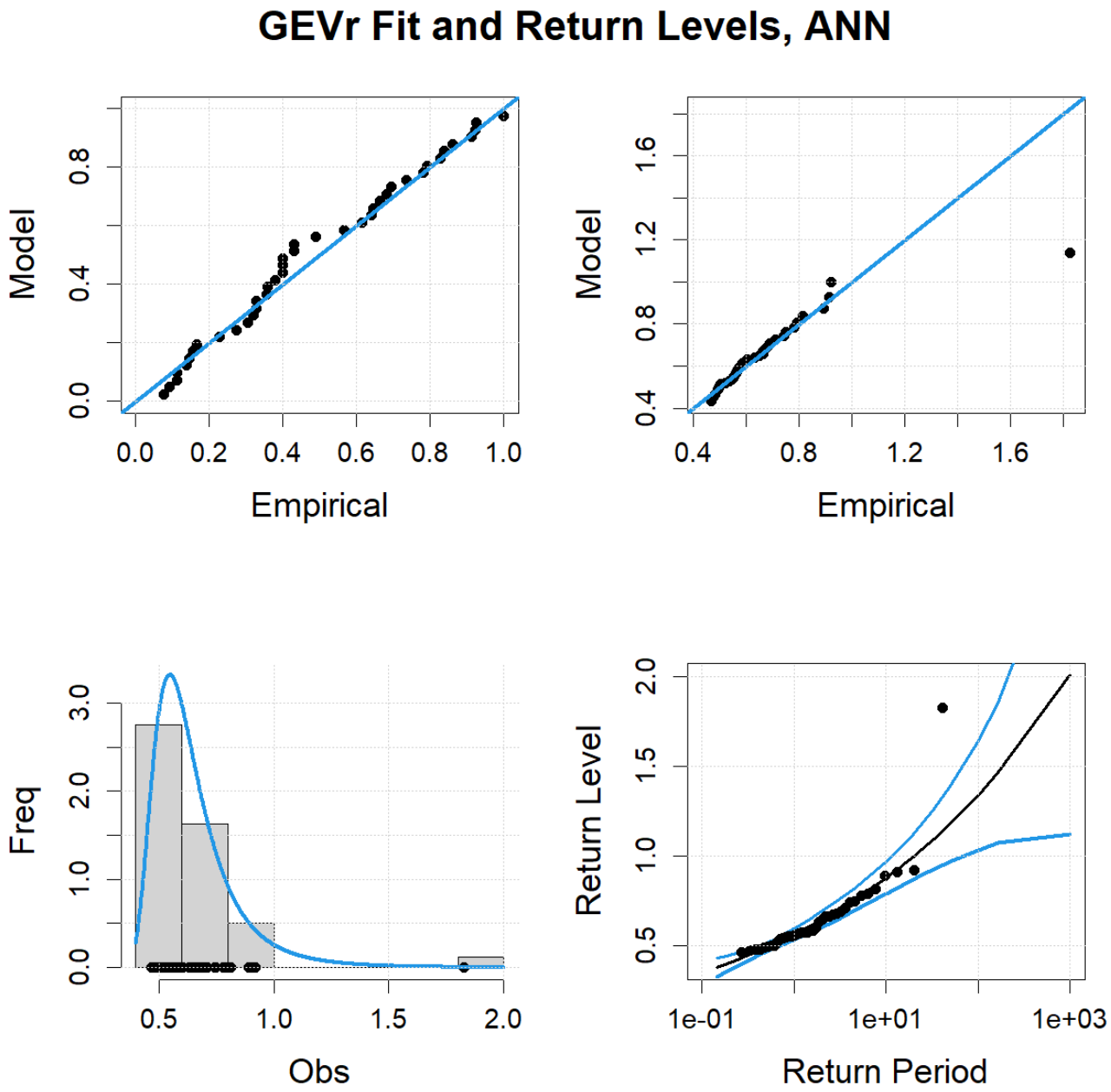

Supplementary Figure 7. Diagnostic plots for extreme skew surge fit to GEVr model at Annapolis NOAA tide gauge (8575512) in the Chesapeake Bay. (see introduction to this supplementary doc for explanation of plots.)

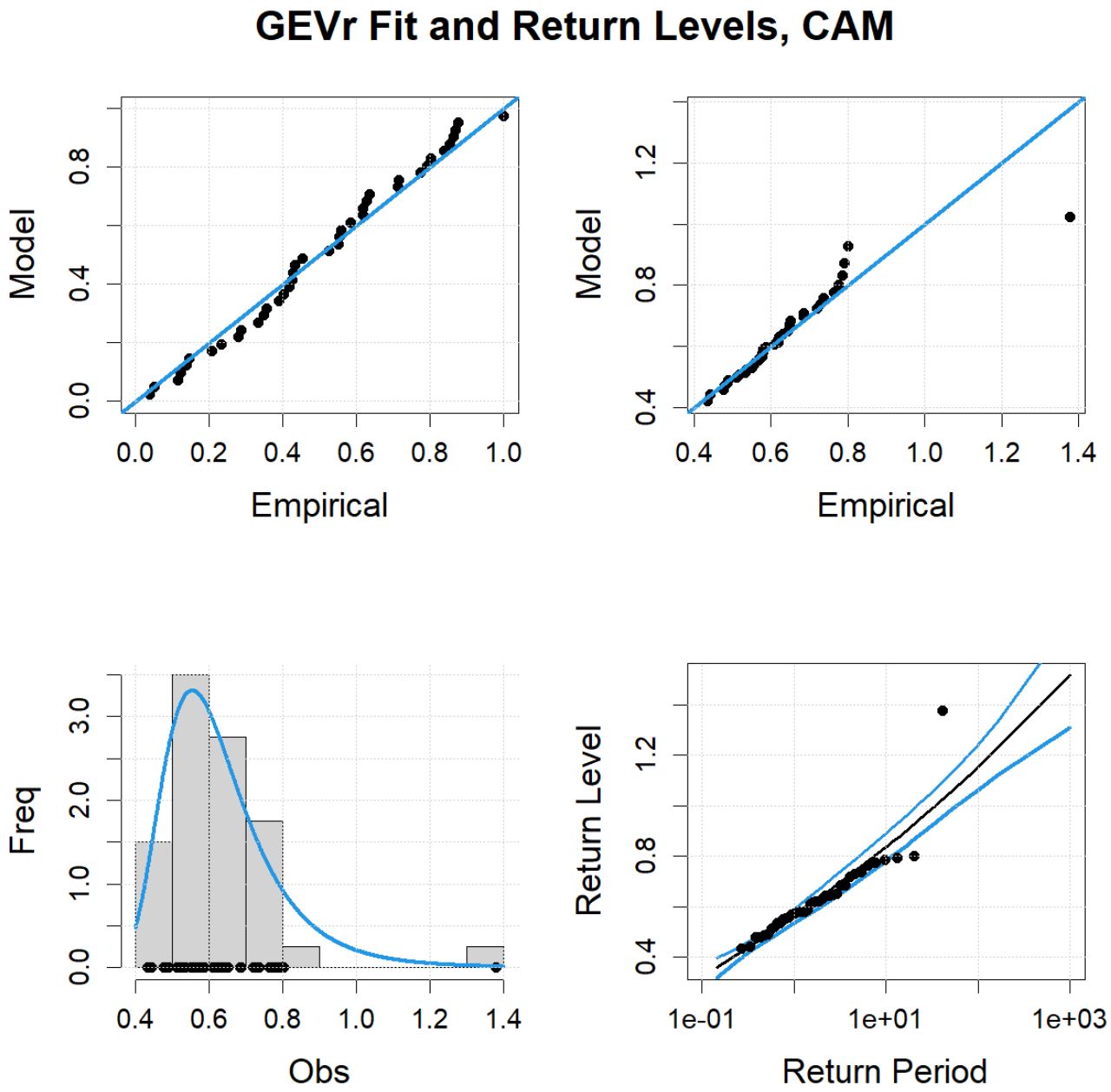

Supplementary Figure 8. Diagnostic plots for extreme skew surge fit to GEVr model at Cambridge NOAA tide gauge (8571892) in the Chesapeake Bay. (see introduction to this supplementary doc for explanation of plots.)

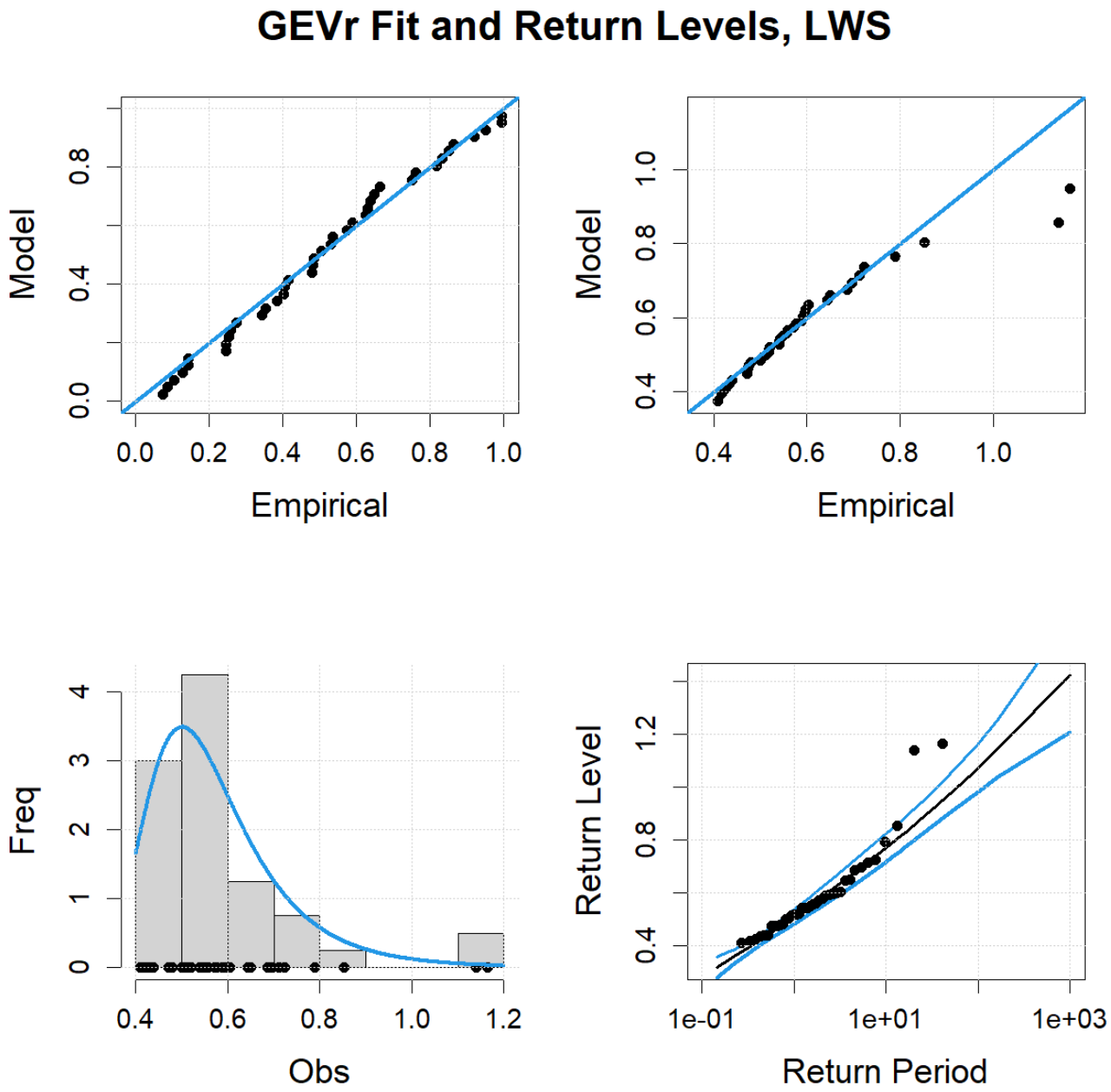

Supplementary Figure 9. Diagnostic plots for extreme skew surge fit to GEVr model at Lewisetta NOAA tide gauge (8635750) in the Chesapeake Bay. (see introduction to this supplementary doc for explanation of plots.)

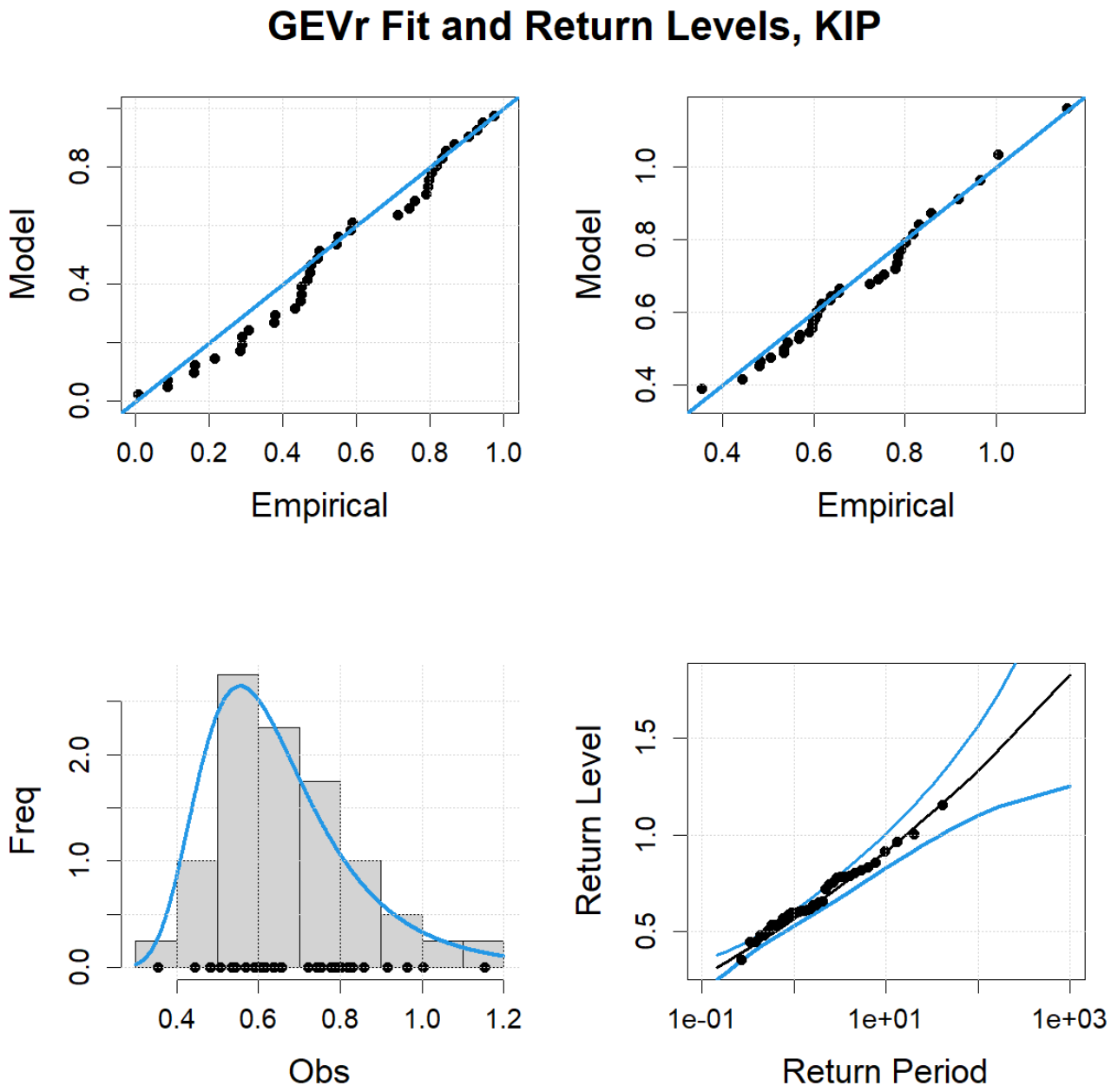

Supplementary Figure 10. Diagnostic plots for extreme skew surge fit to GEVr model at Kiptopeke NOAA tide gauge (8632200) in the Chesapeake Bay. (see introduction to this supplementary doc for explanation of plots.)

Supplementary Figure 11. Diagnostic plots for extreme skew surge fit to GEVr model at Sewells Point NOAA tide gauge (8638610) in the Chesapeake Bay. (see introduction to this supplementary doc for explanation of plots.)

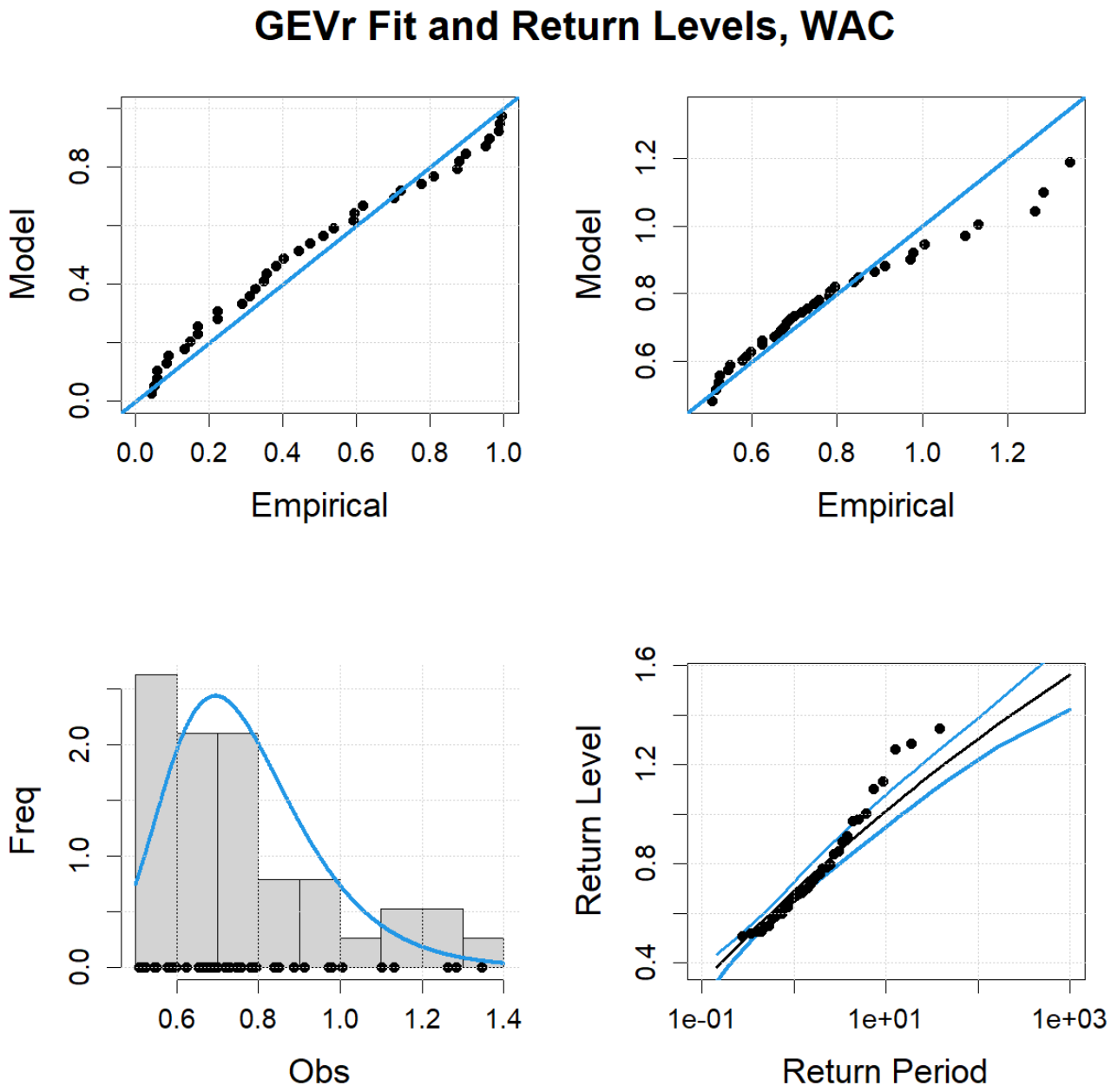

Supplementary Figure 12. Diagnostic plots for extreme skew surge fit to GEVr model at Wachapreague NOAA tide gauge (8631044) near the Chesapeake Bay. (see introduction to this supplementary doc for explanation of plots.)

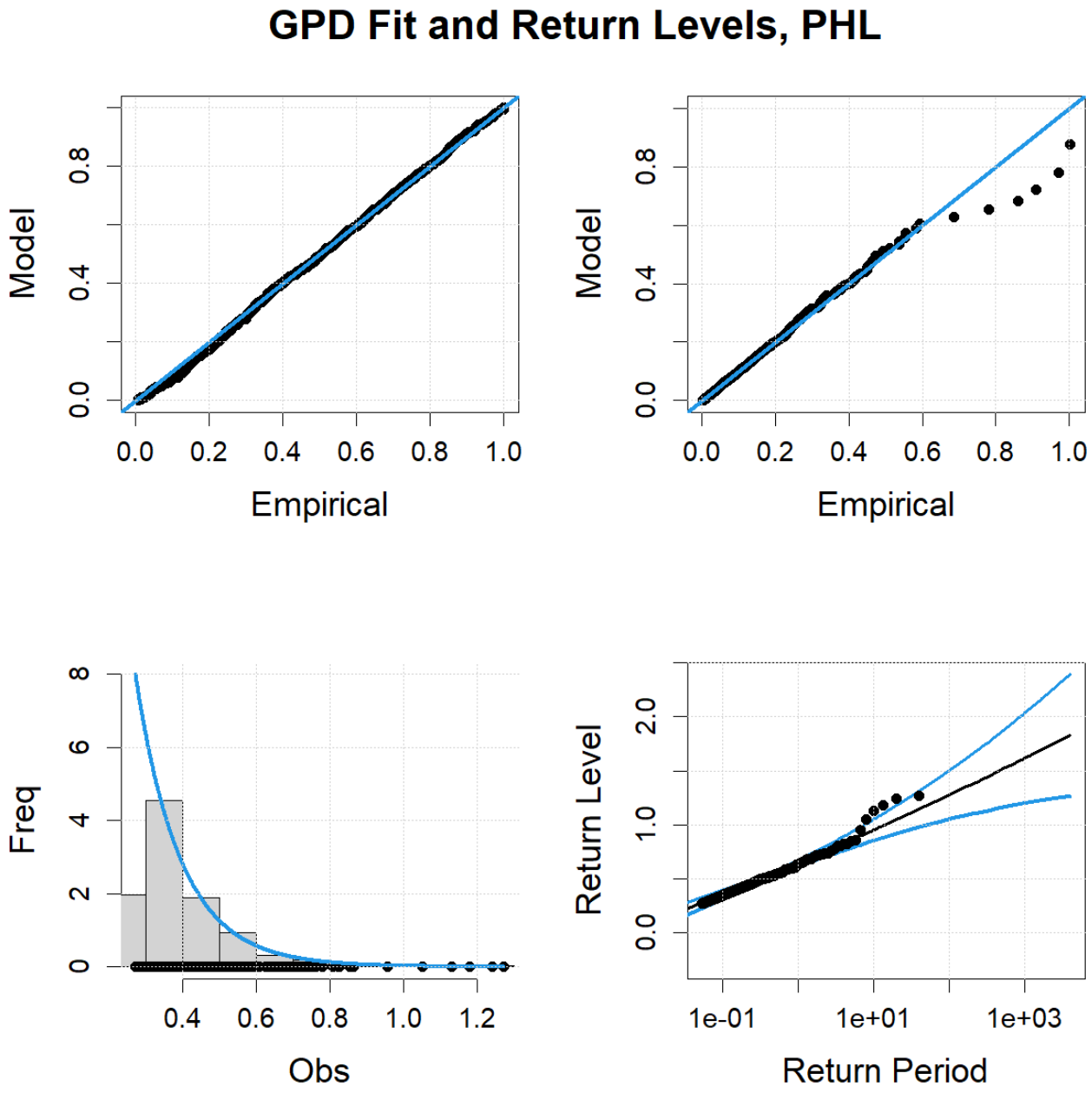

Supplementary Figure 13. Diagnostic plots for extreme skew surge fit to GP model at Philadelphia NOAA tide gauge (8545240) in the Delaware River/Bay. (see introduction to this supplementary doc for explanation of plots.)

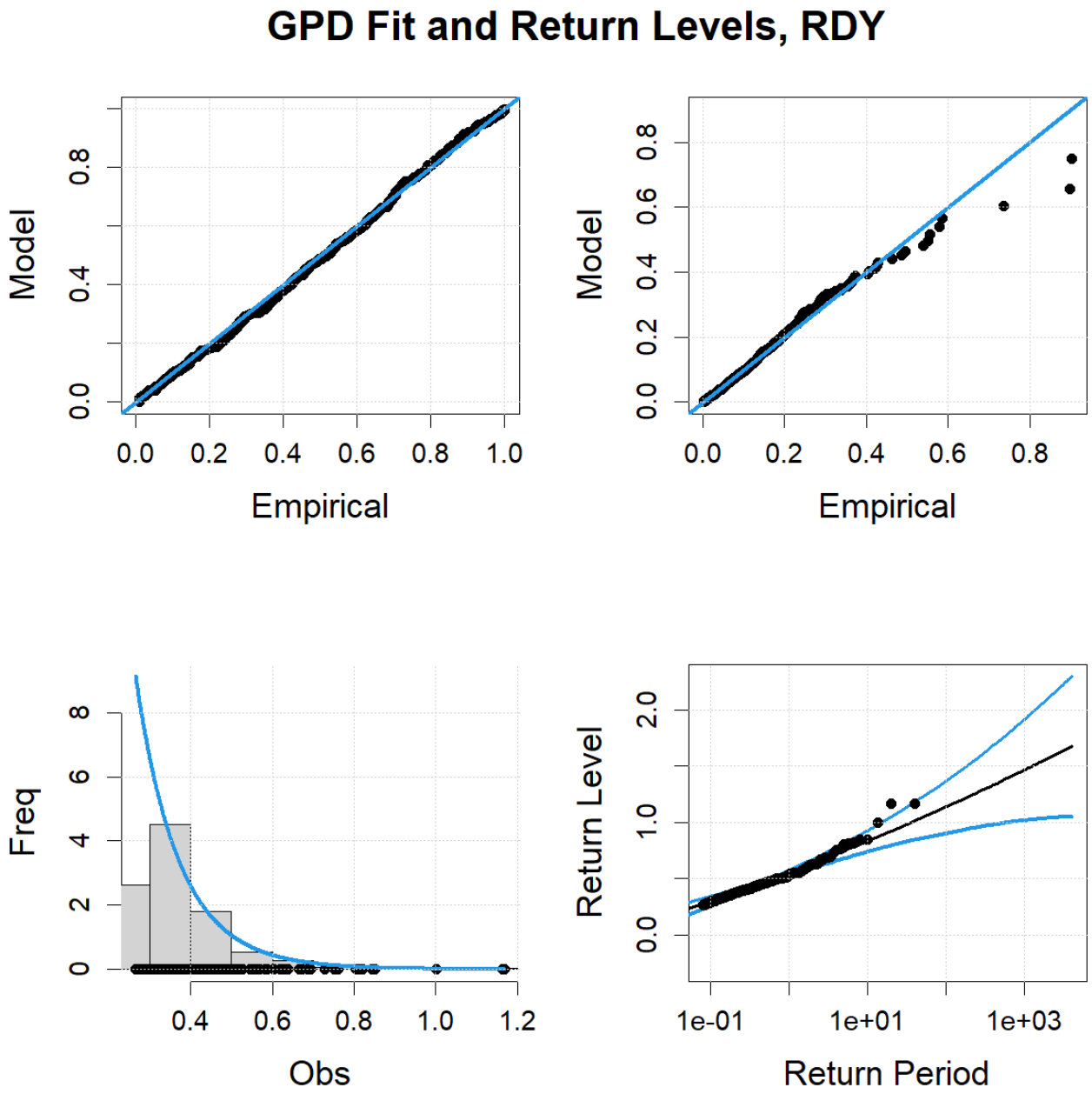

Supplementary Figure 14. Diagnostic plots for extreme skew surge fit to GP model at Reedy Point NOAA tide gauge (8551910) in the Delaware Bay. (see introduction to this supplementary doc for explanation of plots.)

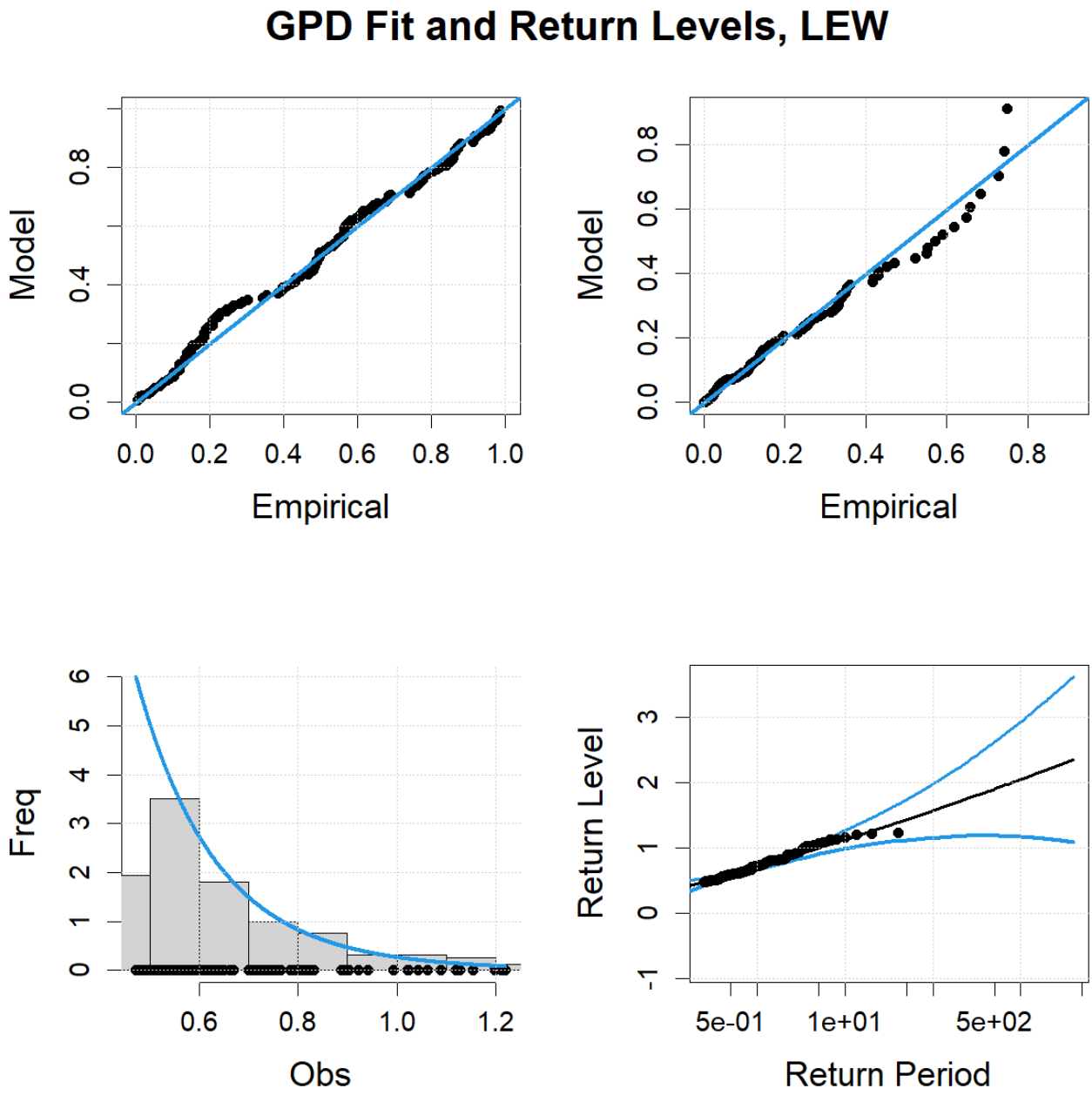

Supplementary Figure 15. Diagnostic plots for extreme skew surge fit to GP model at Lewes NOAA tide gauge (8557380) in the Delaware Bay. (see introduction to this supplementary doc for explanation of plots.)

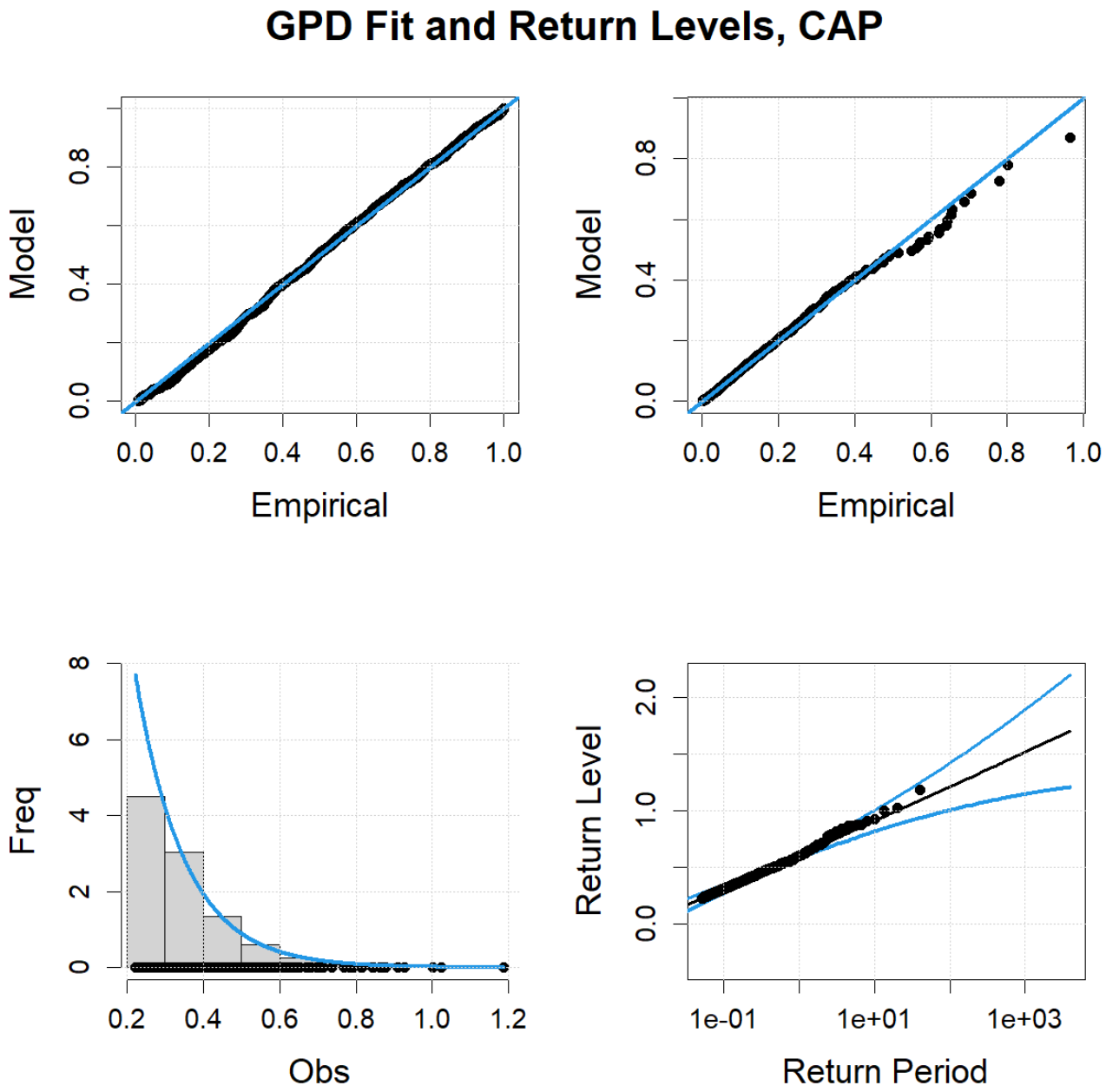

Supplementary Figure 16. Diagnostic plots for extreme skew surge fit to GP model at Cape May NOAA tide gauge (8536110) in the Delaware Bay. (see introduction to this supplementary doc for explanation of plots.)

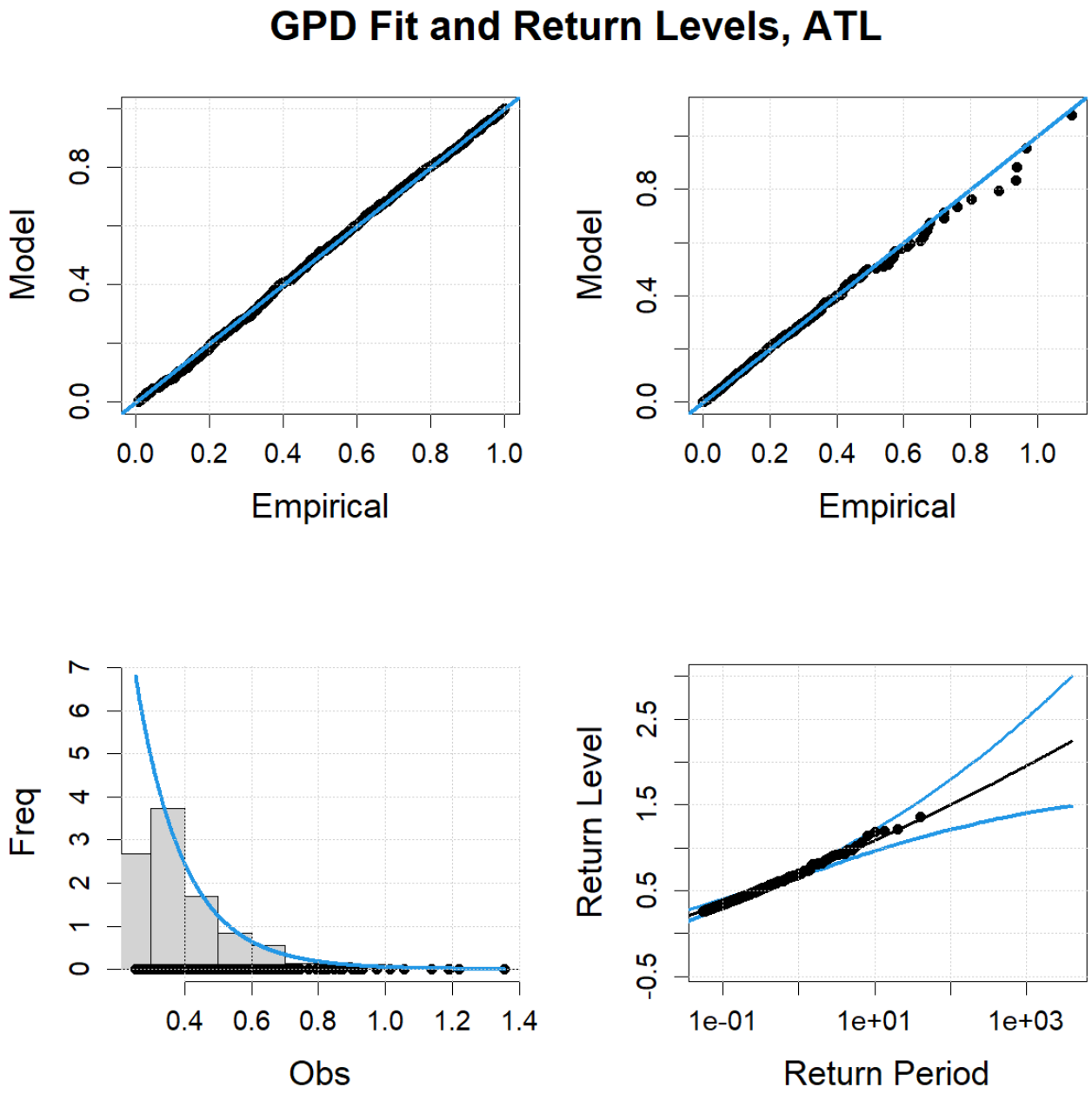

Supplementary Figure 17. Diagnostic plots for extreme skew surge fit to GP model at Atlantic City NOAA tide gauge (8534720) near the Delaware Bay. (see introduction to this supplementary doc for explanation of plots.)

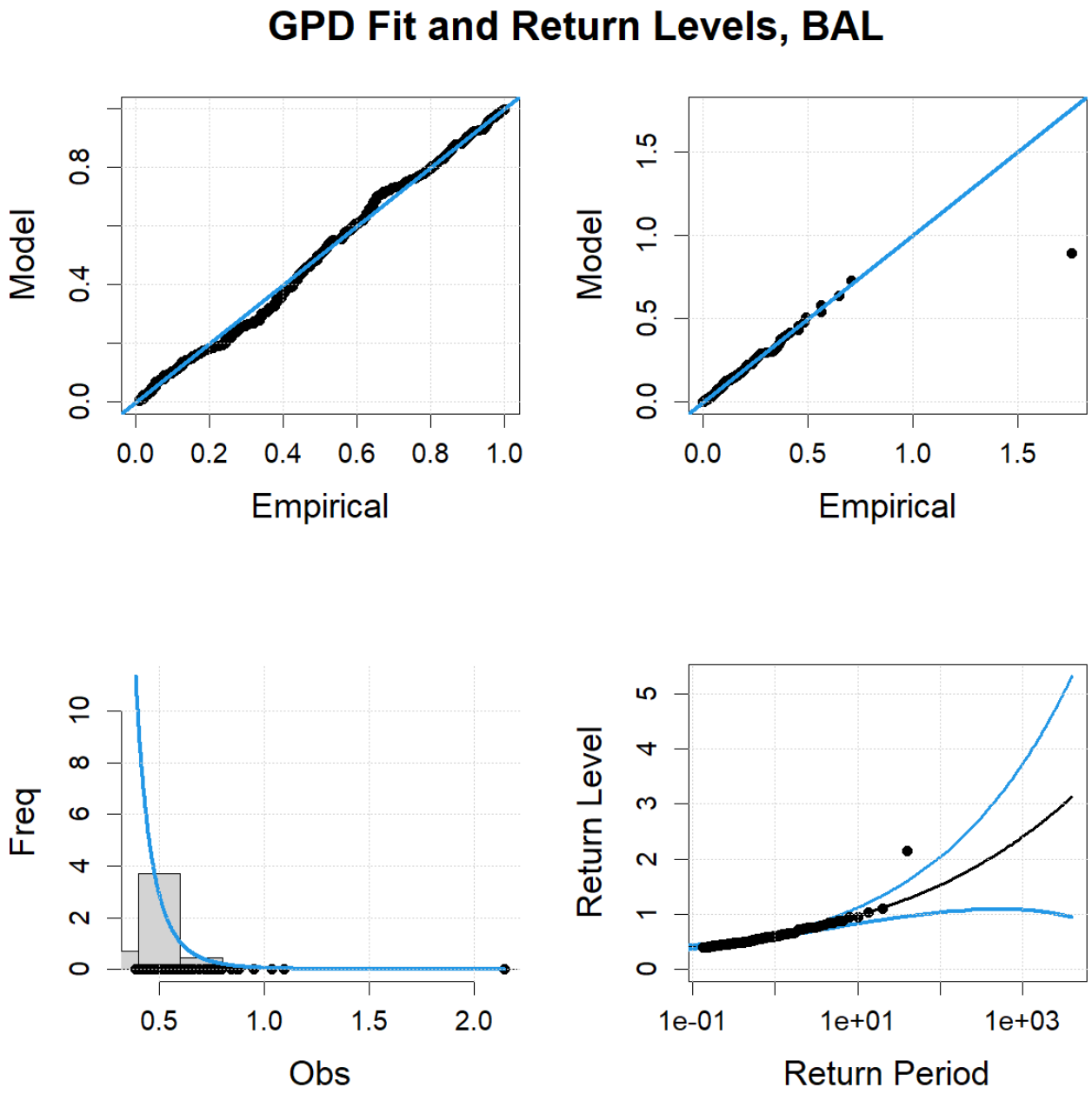

1075

1076 **Supplementary Figure 18.** Diagnostic plots for extreme skew surge fit to GP model at Baltimore
1077 NOAA tide gauge (8574680) in the Chesapeake Bay. (see introduction to this supplementary doc for
1078 explanation of plots.)

1079

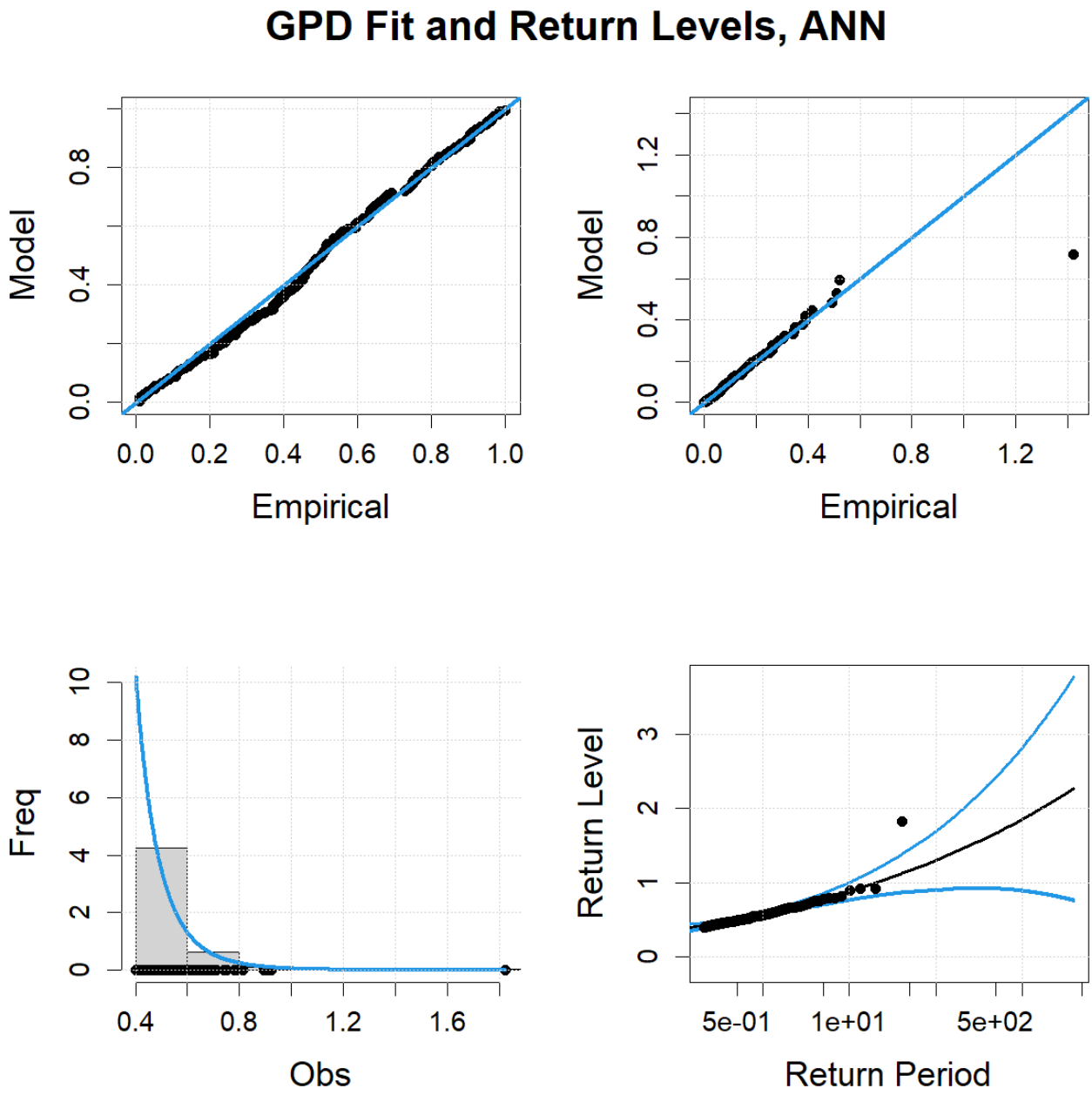

Supplementary Figure 19. Diagnostic plots for extreme skew surge fit to GP model at Annapolis NOAA tide gauge (8575512) in the Chesapeake Bay. (see introduction to this supplementary doc for explanation of plots.)

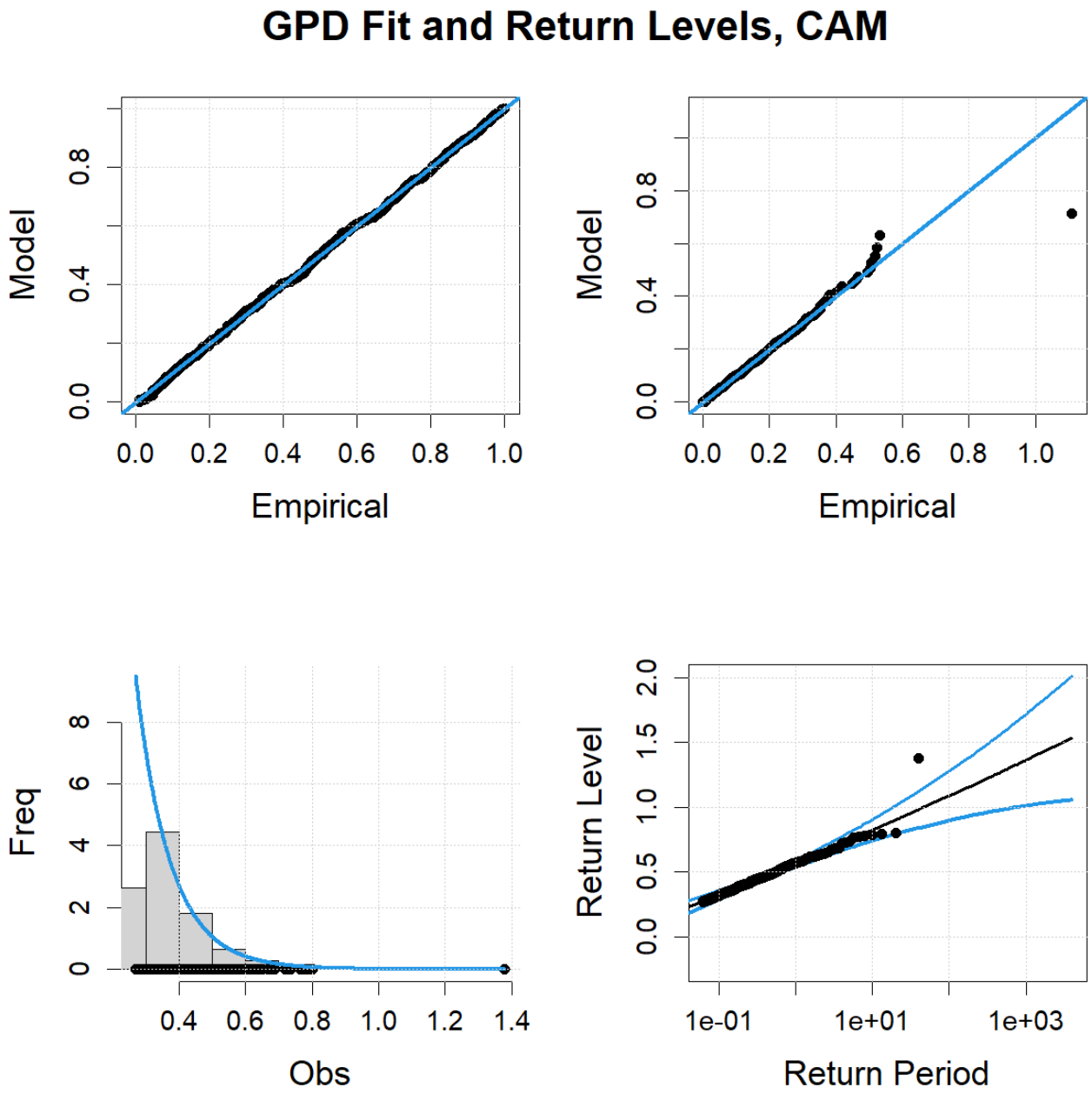

Supplementary Figure 20. Diagnostic plots for extreme skew surge fit to GP model at Cambridge NOAA tide gauge (8571892) in the Chesapeake Bay. (see introduction to this supplementary doc for explanation of plots.)

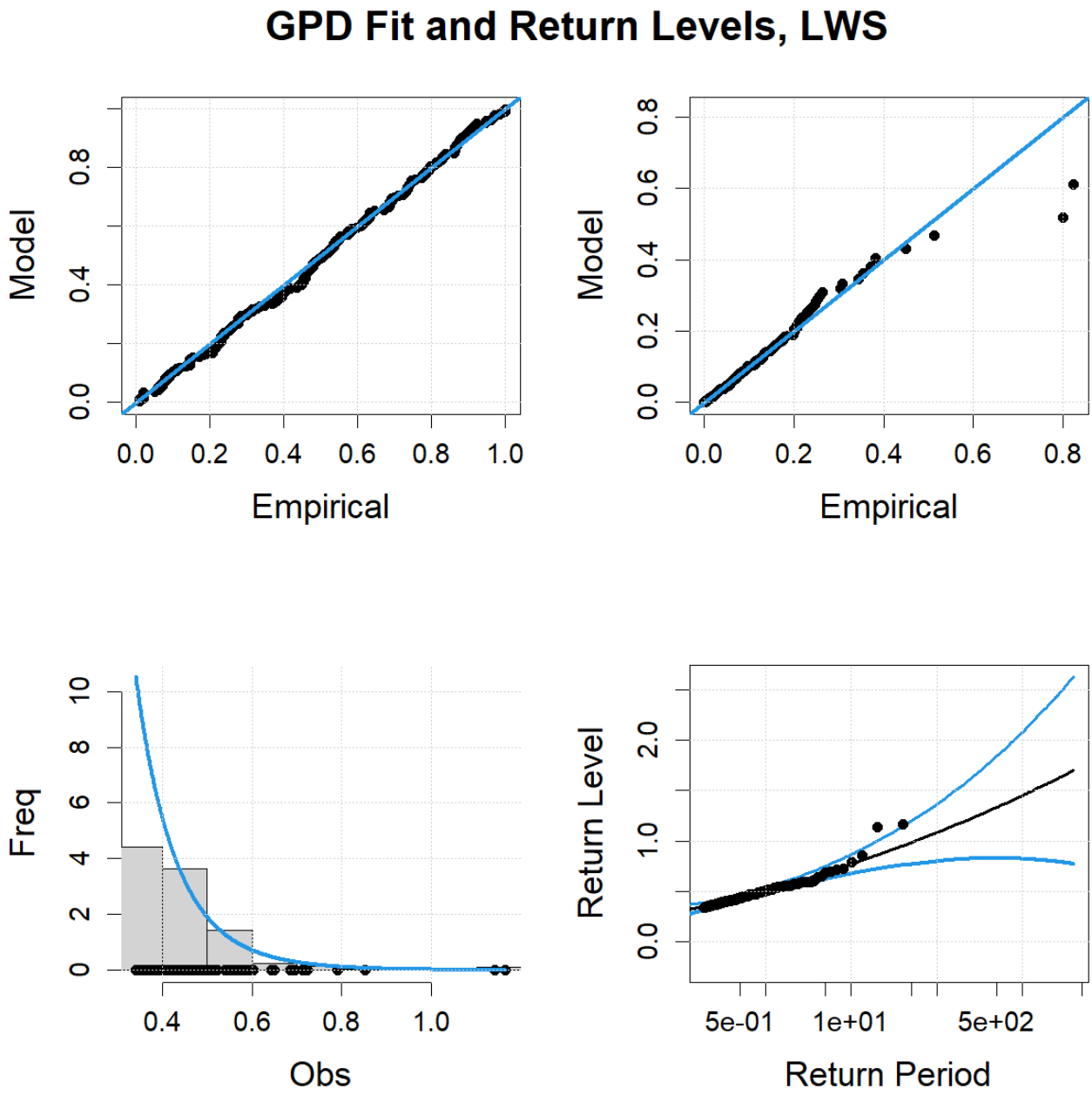

Supplementary Figure 21. Diagnostic plots for extreme skew surge fit to GP model at Lewisetta NOAA tide gauge (8635750) in the Chesapeake Bay. (see introduction to this supplementary doc for explanation of plots.)

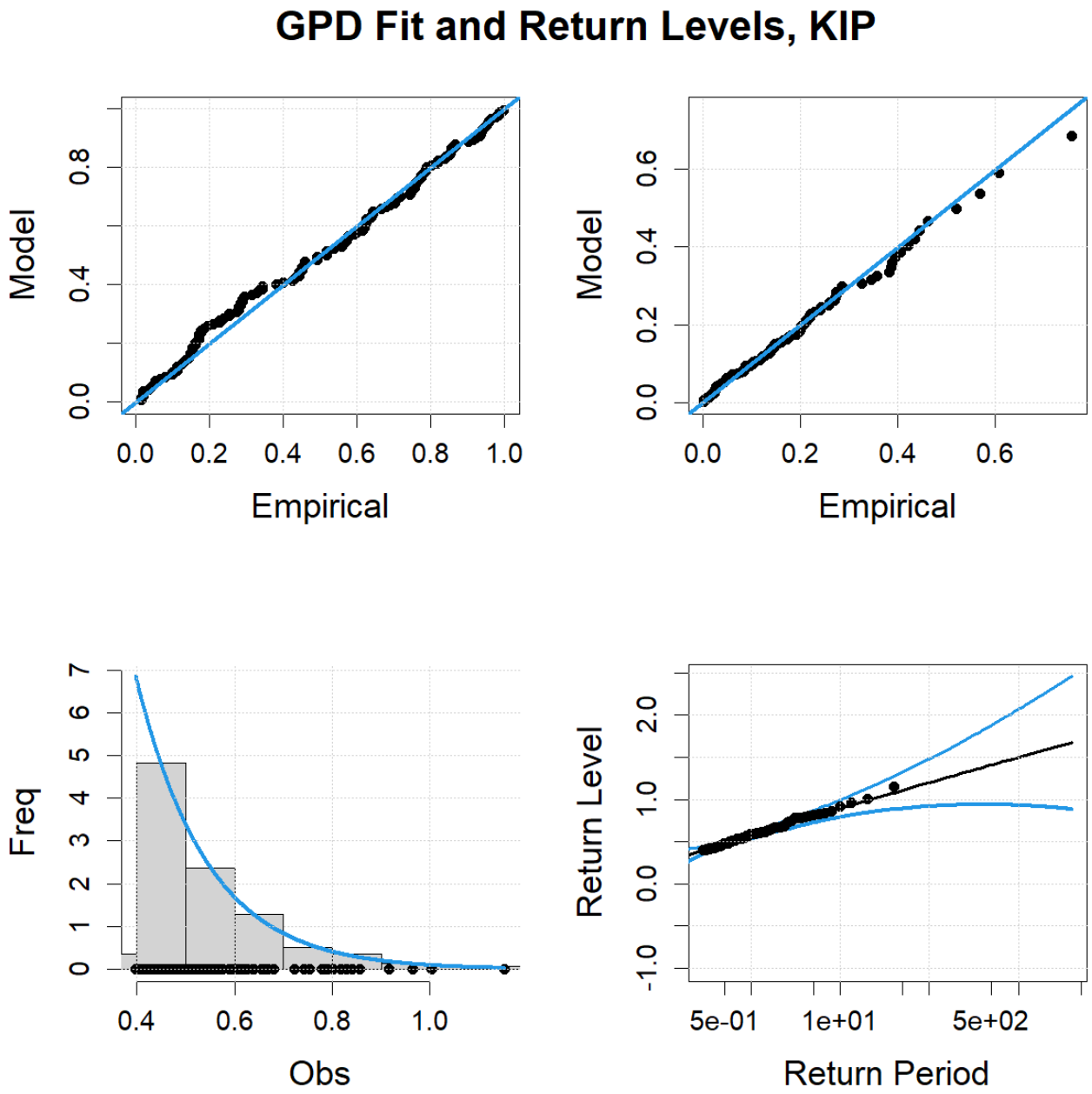

Supplementary Figure 22. Diagnostic plots for extreme skew surge fit to GP model at Kiptopeke NOAA tide gauge (8632200) in the Chesapeake Bay. (see introduction to this supplementary doc for explanation of plots.)

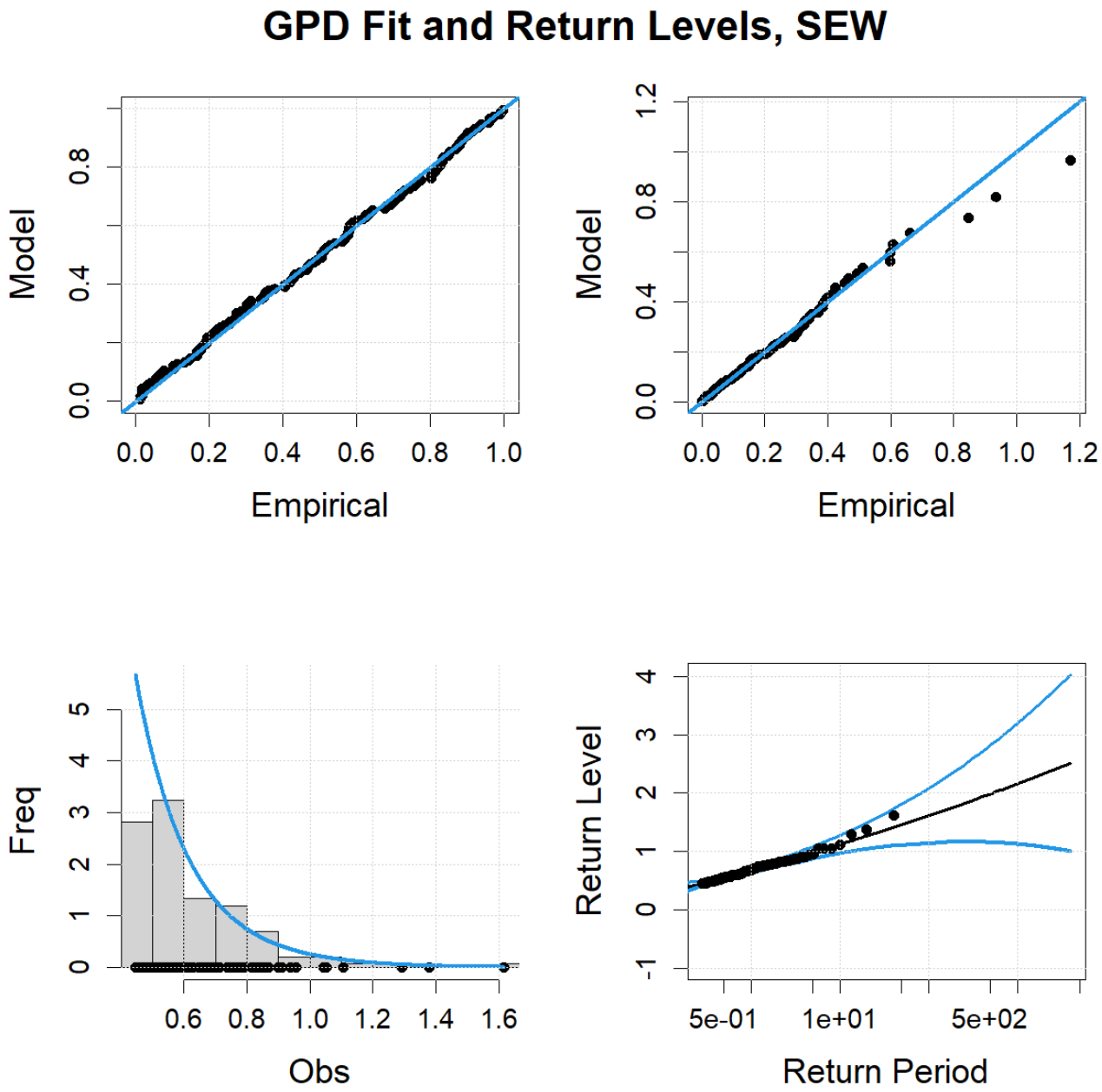

Supplementary Figure 23. Diagnostic plots for extreme skew surge fit to GP model at Sewells Point NOAA tide gauge (8638610) in the Chesapeake Bay. (see introduction to this supplementary doc for explanation of plots.)

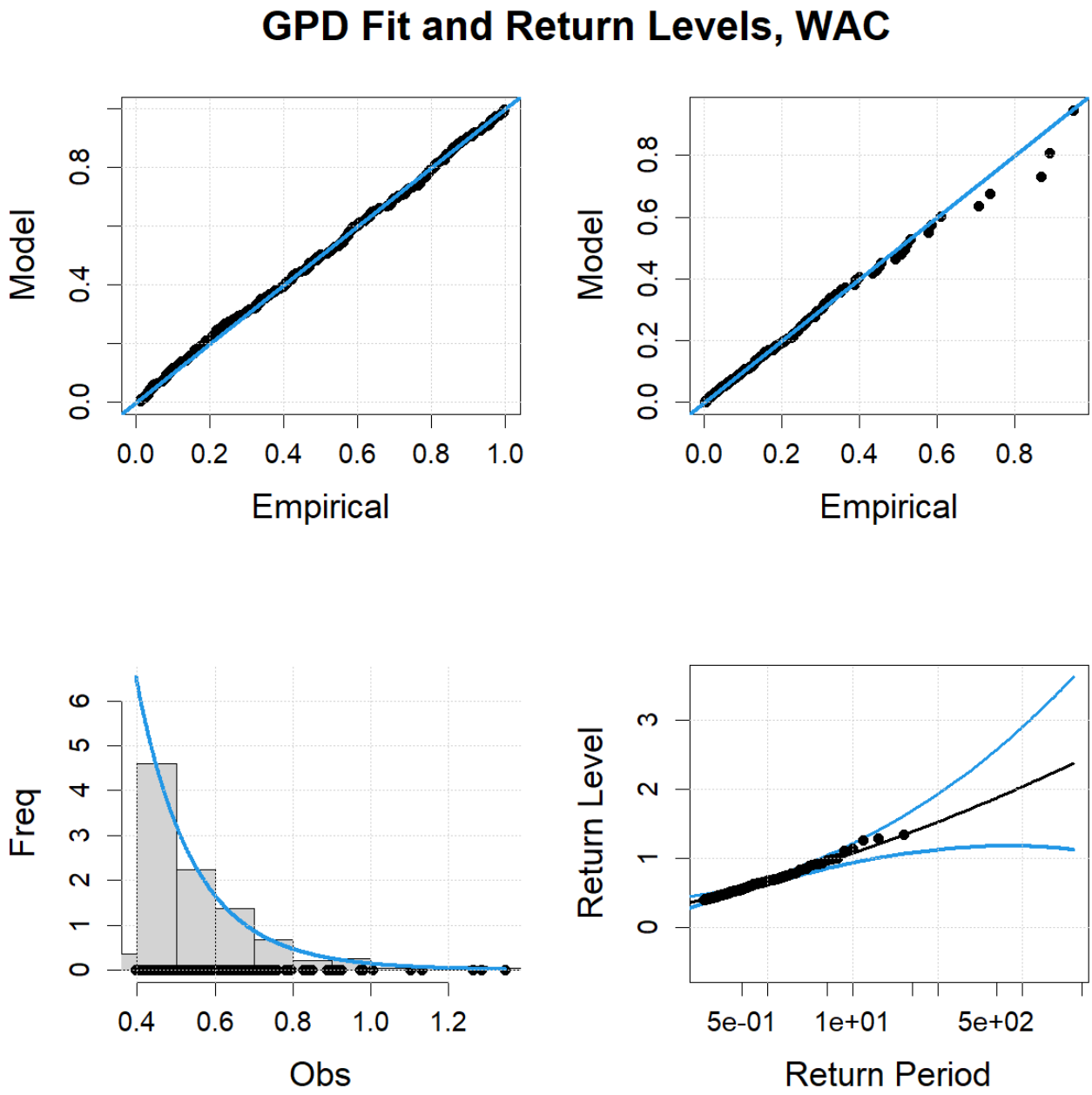

Supplementary Figure 24. Diagnostic plots for extreme skew surge fit to GP model at Wachapreague NOAA tide gauge (8631044) near the Chesapeake Bay. (see introduction to this supplementary doc for explanation of plots.)

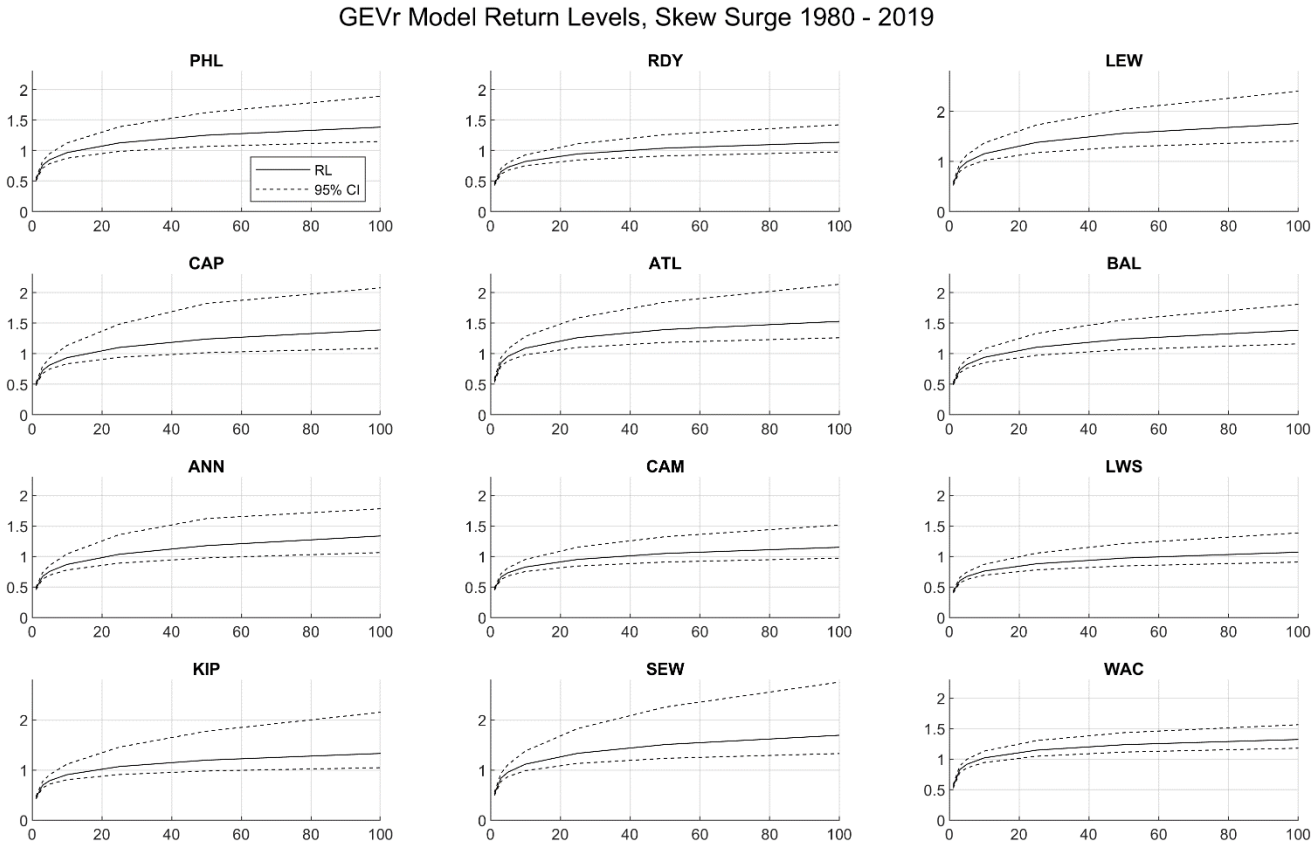

Supplementary Figure 25. Estimates of skew surge for 1.1, 3, 5, 10, 25, 50, 100-year return periods using BM/GEVr approach for tide gauges in the Delaware and Chesapeake Bays, 1980 – 2019. Dotted lines represent upper and lower bounds of 90% confidence interval. Data referenced to NAVD88 meters.

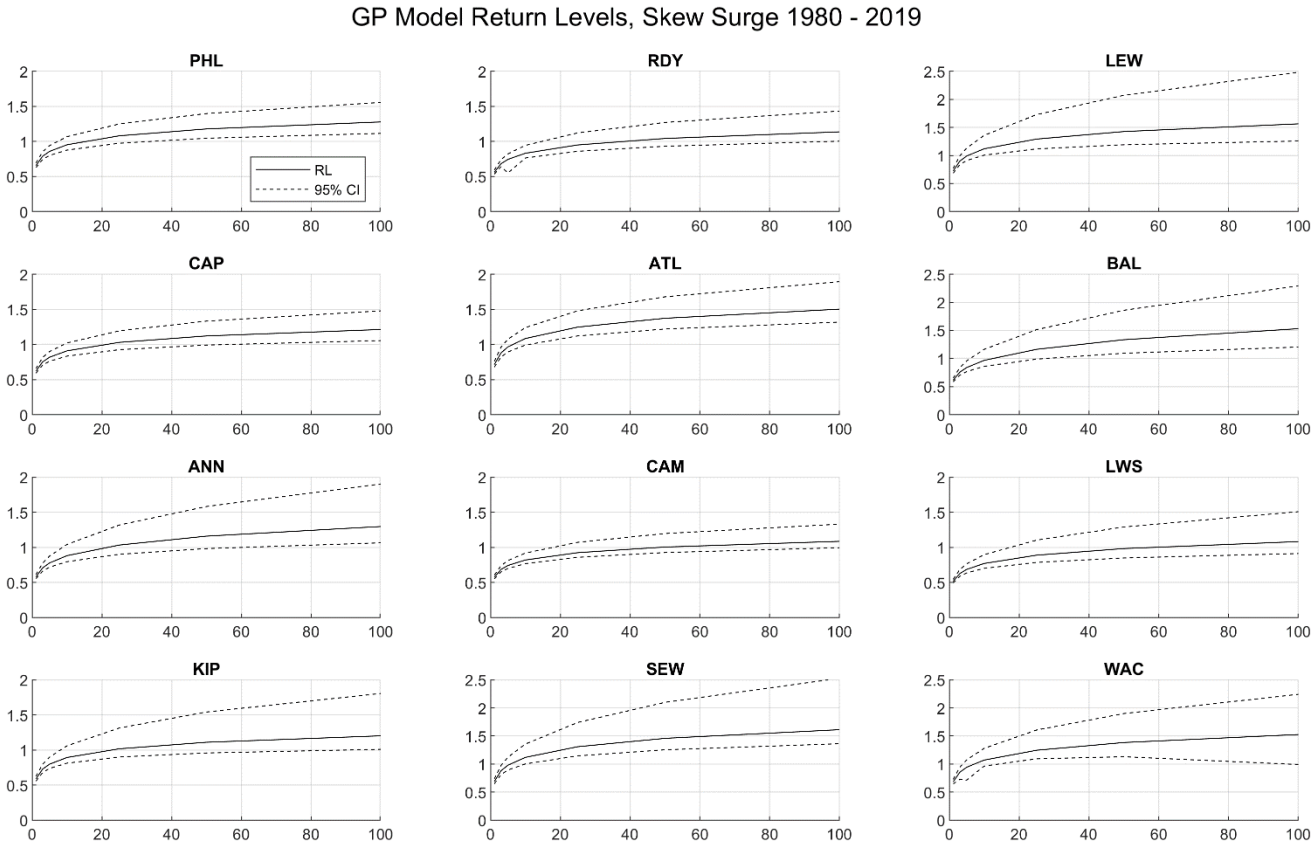

Supplementary Figure 26. Estimates of skew surge for 1.1, 3, 5, 10, 25, 50, 100-year return periods using POT/GP approach for tide gauges in the Delaware and Chesapeake Bays, 1980 – 2019. Dotted lines represent upper and lower bounds of 90% confidence interval. Data referenced to NAVD88 meters.